5-4-2016

Mechanical Stimulation and Stiffness Characterization Device for Electrospun Cell Culture Scaffolds

Soliman A. Alhudaithy
saa14009, soliman.alhudaithy@uconn.edu

Mechanical Stimulation and Stiffness Characterization Device for Electrospun Cell Culture Scaffolds

Soliman Abdullah Alhudaithy

B.S., King Saud University, College of Applied Medical Sciences, Biomedical Technology, 2011

A Thesis
Submitted in Partial Fulfillment of the
Requirements for the Degree of
Master of Science
At
University of Connecticut

2016

APPROVAL PAGE

Master of Science Thesis

Mechanical Stimulation and Stiffness Characterization Device for Electrospun Cell Culture Scaffolds

Presented by,

Soliman Abdullah Alhudaithy, B.S.

Major Advisor	Kazunori Hoshino, PhD
Associate Advisor	Guoan Zheng, PhD
Associate Advisor	Quing Zhu, PhD

University of Connecticut
2016

Acknowledgements

First of all, I praise and thank God Almighty for His blessings. Unforgettably, thanks belong to my father Prof.Abdullah Alhudaithy, my mother Prof. Amal Alshawi, siblings Norah, Nouf, Layla, Mossaed as well as my nephew Khalid and neice Hatoun for their continuous support, guidance, sacrifices, and love.

I am incredibly grateful and lucky that my major advisor is prof. Kazunori Hoshino, as he encouraged me the most to accomplish a lot towards my goals under his professional guidance, efforts, support, knowledge, and advice. Thankfully, I will be completing my education journey with his great supervision and personality.

I would like to thank my committee members, Prof. Quing Zhu, and Prof. Guoan Zheng, for their guidance and assistance. Acknowledgement to prof. Sangamesh Kumbar, and Dr. Namdev Shelke at University of Connecticut Health Center for their collaboration and help.

Special recognitions to my sponsor, King Saud University, the Saudi Arabian Cultural Mission, and my fellows for their substantial support, understanding, and encouragement.

My colleagues at the University of Connecticut, Devina Jaiswal, Hassan Fiaz, Radhika Shiradkar, Mohammed Alharthi, Mohammed Ba Rajaa, David Kaputa, G. Alexander Korentis, Kaikai Guo, Mengzi, Mengdi, Zichao Bian, Zhe, Jun, Amanda, and Yuji thank you all for being there and for your support during my studies.

My friends and beloved ones, either acknowledged here or not thank you for being in my life, that alone was another factor towards my success. I know words are insufficient to express my appreciation for all of you. Thanks again.

Table of Contents

Title Page i
Copyright Page ii
Approval page iii
Acknowledgements iv
Table of contents v
List of Figures vi
List of Tables vii
List of Charts vii
Abstract viii
Chapter One - Introduction **1**
1.1 Thesis Outline 1
1.2 Background and Motivation 2
1.3 Aims of Thesis 6
Chapter Two - Methods **7**
2.1 A Description of the Device Function and Design 7
2.1.1 Principle of Operation 8
2.1.2 Design Considerations 10
2.2 Continuous Strain Measurements and Force Correlation 11
2.2.1 Strain Gauges and Digital Microscopic Setups 11
2.2.2 Laser-Based Optical Lever Sensing of Spring Bending Forces 13
2.3 Equations Used to Characterize Materials Mechanical Properties 16
2.4 Fabrication and Materials 20
2.4.1 3D Printed Assemblies and Subassemblies. 20
2.4.2 Leaf Springs Fabrication. 22
2.4.3 Electrospinning nanofiber polymer substrates 25
2.5 Calibration Method 27
Chapter Three - Results **28**
3.1 Equivalent Spring stiffness k_1, Young's Modulus E_1, and Sensors' Calibration Relationships 28
3.2 Nanofiber Polymer Substrates' Measured Mechanical Properties 29
Chapter Four - Conclusion **34**
4.1 Sensors Calibration Discussion 34
4.2 Polymer Testing Discussion 34
4.2.1 Our Device Results 34
4.2.2 Our Device Results Compared to Instron Results 35
4.3 Future Work 36
References **37**

List of Figures

Figure 1: Instrument design isometric view (with section cuts). ..... ……...7
Figure 2: Active arms in the system (left image shows immersed active arms in media) 8
Figure 3: (A) System initial equilibrium state, (B) System deformed by force F, and (A1) represents (A) while (B1) represents (B) in the corresponding spring schematic diagrams.....9
Figure 4: (A) Parallel leaf spring configuration and parameter definition. (B) Wheatstone half bridge representative circuit. (C) Parallel leaf springs showing strain gauges' attachment. (D) Simulation showing the maximum stress points….....…… 11
Figure 5: (a) Mirror like reflection with no offset and no tilt angle. (The X-axis is the mid-length of the leaf spring)……...…...…….……13
Figure 5: (b) Mirror like reflection with offset and no tilt angle Øº, (dashed red line is the initially reflected spot when F=0, solid red line is displaced on PSD by d1)…….……...…… 14
Figure 5: (c) Mirror like reflection with offset and tilt angle Øº, (dashed red line is the previously reflected laser spot [fig 5, a &b], Solid red line is displaced by d1+d2)……...…….. 14
Figure 6: Defining dimensional parameters. (a) Target side view. (b) Top view of the elongated specimen…….…...16
Figure 6: Maximum tilt angle area simulation…….……..…..……19
Figure 7: Polyamide 3D printed assembly…….…….……..20
Figure 8: (a) Substrate holders attached to polymer substrate and ready for testing. (b) Detached individual parts of the installation kit (c) actual polymer installation kit…….…….…..……21
Figure 8: polymer Installation kit attachment to active arms (d) before installation (e) during installation (image from opposite side), (f) after installation to active arms……..……..22
Figure 9: (a) Metal sheet-photoresist sandwich lamination & their side view……..23
Figure9: (b) Photomasks alignment & their side view……..23
Figure 9: (c) Ultraviolet photolithography Patterning……...…….……23
Figure 9: (d) Photoresist Development, metal etching, and final product…….24
Figure 10: (a) Fabricated leafs (b) Half polished and scratched springs, the left leaf is reflecting room light……...……....24
Figure 11: (a) Electrospinning fabrication principle, (b) Electrospinning fabrication setup…….…...25
Figure 12: (a) shows a zoomed view of the polymer substrate surface (b) Custom-made polymer substrate cutter blade ……..……....…26
Figure 13: tested specimens in petri dish, a specimen ready for installation (middle) and detached polymer installation kit……...……...……26
Figure 14: Calibration method (force towards gravity) (a) illustration of calibration, (b) actual flipped sensors calibration…….…….…...….27
Figure 15: Nano fibrous scaffold (SEM micrograph) seeded with MCF-7 cancer cells showing cellular attachment to fibers (inset)……...36

List of Tables

Table 1: Polymer substrate samples' dimensions mechanically tested……..…...26
Table 2: Elastic moduli of tested polymers of different composition……...…….34

List of Charts

Chart1: Spring 1 calibration (A) Force-elongation (stiffness) curve (B) Force-bridge relationship (C) Force-PSD relationship (D) elongation-PSD……..……..……...28
Chart 2: (a) PCL 100 Young's modulus……...…….29
Chart 2: (b) PCL:CA 95:5 Young's modulus……...…….30
Chart 2: (c) PCL:CA 90:10 Young's modulus…….….30
Chart 2: (d) PCL:CA 80:20 Young's modulus……..……31
Chart 3: (a) PCL 100 Stiffness test results (Instron results: 3 samples average in orange and their deviation in black bars), (our device results: in blue)…….….32
Chart 3: (b) PCL:CA 95:5 Stiffness test results (Instron results: 3 samples average in orange and their deviation in black bars), (our device results: in blue)……..32
Chart 3: (c) PCL:CA 90:10 Stiffness test results (Instron results: 3 samples average in orange and their deviation in black bars), (our device results: in blue)…….……33
Chart 3: (d) PCL:CA 80:20 Stiffness test results (Instron results: 3 samples average in orange and their deviation in black bars), (our device results: in blue)…….……33

Abstract

Mechanical stimulation of in vitro tissues showed a huge potential in studying cell mechanics and their related regenerative tissue engineering applications. This thesis proposes a device that applies measurable uniaxial longitudinal tensile forces to 3D tissue engineered polymer substrates, under cell culture environment, for mechanical properties characterization. Stiffness characterization of substrate polymers is important since they form the mechanical transduction scheme to cultured cells. The device measures the stiffness of substrate polymers by continuously monitoring their elongation in real-time due to (<0.5N) applied forces.

In this study, Poly-ε-caprolactone (PCL) and Cellulose Acetate (CA) nanofibers of different solution composition were electrospun and mechanically tested. The measured elastic modulus of PCL 100, PCL:CA 95:5, PCL:CA 90:10, and PCL:CA 80:20 was 8.96 N/mm², 10.61 N/mm², 12.39 N/mm² and 17.66 N/mm², respectively. The obtained results follow literature where they show an increase in the electrospun substrates' stiffness with CA % increase.

Chapter One

Introduction

1.1 Thesis Outline

Chapter one starts with a thesis outline; then provides an overview of the literature applicable to this research. The first section relates some diseases with cellular mechanics, then shows the importance of some approaches that have been used to explore the mechanical properties. The background also reviews the effects of different external stimulation as factors in various bio-applications as they demonstrate the significance of further investigation. The first chapter ends by stating aims of the thesis.

Chapter two starts with a description of the proposed device and its principle of operation; then it briefly covers the theories and scientific formulas that the device obey. Then, the chapter includes the approach employed in the fabrication process, the materials used, and the calibration method. The experimental setup images are shown next to the explanation illustrations when applicable.

Chapter three provides the biosensors calibration results, the experimental measured and calculated mechanical properties of four polymer substrates (by our proposed device and Instron 5544 for material mechanical testing).

Chapter four provides the consequence conclusion of this research then carry the related discussion, and specifies some future related work.

1.2 Background and Motivation

The history of research in studying the mechanical characteristics of cells and tissues started decades ago, but recent advancement to conduct real-time analysis in the field did not exist by that time. The starting point and growth of some human disease conditions can be extensively associated with the mechanical properties of cells and tissues. Some deviations in the mechanical properties of the cells can disrupt their physiological functions causing diseases like malaria (1). Similarly, diseases may result in changes in the mechanical and morphological properties of living cells and tissues like cancer (2). In human disease studies, an essential role player in distinguishing diseased cells or tissues from healthy ones is cell mechanics (3). Ever since it has been investigated and recognized that diseases like cancer can alter the cells' mechanical properties, such studies will likely assist in the early detection of cancer (4). Furthermore, studying the mechanical properties of cancer cells helped to understand the physical mechanisms in charge of cancer metastasis.

Latest progression in biomechanics has resulted in the opportunity of exploring mechanical influences on cells, but there are few experimental techniques capable of determining the mechanical properties of cells (5). Another branch of mechanical properties' studies depends on the external influences like mechanical stimulation to the cell culture. It plays a substantial role in cell differentiation, proliferation, and connective tissues maintenance when it subserves a mechanical function (6, 7). Mechanical stimulation also has other effects like mesenchymal stem cell lineage commitment signaling (8).

Rajagopalan J and Saif (9) reviewed the importance of various mechanical properties' studies were and microenvironments on the cellular level and their impact on cellular procedures

like cell differentiation, locomotion, development, and growth (10-12). Likewise, in vitro cell behavior across a variety of cell types is influenced by externally applied forces that alter various aspects (13-15).

The mechanical microenvironment shows a significant role in fibroblast migration throughout wound healing (16), synaptic neurons plasticity regulation (17), and tumor cell response regulation (18). It is essential to understand how cells sense and generate forces and how these forces are transduced into biochemical signals for better comprehension of cell behavior in both normal and pathological states (19, 20). Therefore, precise measurements of displacements and forces produced by cells and to the cells are necessary for both in vivo and in-vitro studies (21).

Gillispie JS studied the electrical and mechanical activities of smooth muscle cells of the intestine and their responses to sympathetic nerve stimulation (22). Moreover, Burnstock G, Holman ME have reported similar research (23, 24), studying the smooth muscle of guinea-pig vas deferens and the hypogastric nerve. In the same year, Burnstock & Prosser studied the smooth muscle's quick stretch response and the stretch relation to conduction (25). Later, Leung DYM et al. investigated the effects of cyclic stretching on smooth muscle cell biosynthesis, and their results showed higher protein and collagen synthesis under stretch while DNA under more agitation (26). Then, Burchiel KJ studied the effects of electrical and mechanical stimulation of the neuroma; the tetanic electrical stimulation created either a change in the starting point of firing rate or elongated after-discharges in fibers demonstrating an activity of neuroma (27). On the other hand, mechanical stimulation of the neuroma formed both prolonged after-discharges and short-term increases in spontaneous discharges. Two years later, Grigg P published a paper explaining how mechanoreceptor stimulation leads to opening the mechano-sensitive ion channels and produce a

transduction current that changes the cell membrane potential (28). Sanderson et al. concluded that mechanical stimulation with the presence of intercellular communications to ciliated cells of the respiratory tract in culture has induced a wave of rising Ca^{2+} which propagates cell by cell and reached the neighboring cells demonstrating a mechanotransduction effect (29).

Delbono et al. determined that calcineurin has a possible relation between growth and mechanical loading because insulin-like growth factor (IGF)-I stimulus of muscle fibers can cause increases in cytosolic Ca^{2} +, partially because of increased L-type Ca^{2+} channel activity (30). Also, since calcineurin is activated by calmodulin that has bound calcium; thus, its activity is mostly controlled by cytosolic calcium concentrations' changes (31).

In the field of tissue engineering and regenerative medicine, many studies established the benefits of electrical and mechanical stimulation for cell culture applications such as bioscaffolds, tendons repair, polymer constructs, cell attachment and proliferation. In regards to electrical stimulation, Wong JY et al. discussed the surface properties of electrically conducting polymers like charge density and wettability, they can be reversibly changed using an applied electrical potential. Their results propose that electrically conductive polymers can represent a type of culture substrate which could provide a noninvasive means to control the function of adherent cells as well as their shape, without any medium alteration (32).

Function and growth of cultured cells are usually controlled by adding medium supplements, including serum, soluble hormones, and defined growth factors. Nevertheless, cells and their culture substrate interactions are also critical for regulation of their function and growth. For instance, the majority of mammalian cells depend on anchorage, therefore, must attach and spread on a surface to proliferate (33-37). Numerous culture substrate analysis has shown that surface charge density, wettability, and morphology are vital to controlling cell attachment,

function, and metabolism (38). Polymers that are electrically conductive offer potentially attractive surfaces for cell culture in regards to their surface properties as they can be reversibly altered by electrochemical or chemical oxidation or reduction (39, 40). Likewise, Schmidt showed the outgrowth of neurite when subjected to electrical stimulation on a conductive polymer (41).

Regarding mechanical stimulation, Kim et al. found that the application of short-term cyclic strain increased proliferation engineered smooth muscle cells on different polymeric scaffolds (42). On the other hand, the application of long-term cyclic strain upregulated collagen gene expression, elastin, and raised tissue organization. Moreover, Dennis E. confirmed that tissue cells respond to the stiffness of their substrate by external mechanical stimulation (43). Brown TD discussed several techniques of mechanical stimulation of cells. He categorized different mechanical stimuli setups based on their primary loading modality; the categories covered were compressive loading, longitudinal stretching, substrate bending, out of plane circular substrate distention, in plane substrate distention, specialized distension, fluid shear systems as well as combined fluid shear with distention systems (44).

To summarize, many studies show tremendous potential for further mechanical characterization of externally applied forces to cell culture substrates as well as real-time monitoring of cell growth and response. Since the polymer substrate is the scheme for mechanical stimulation transduced to cultured cells, this scheme needs to be characterized in terms of mechanical properties in order to further investigate attached cells' mechanics.

To this extent, this research intends to study the longitudinal stretching effects of tissue engineered polymer substrates for stiffness measurement and characterization.

1.3 Aims of Thesis

- The goal is to build a cell culture microenvironment friendly device that applies measurable uniaxial longitudinal tensile forces to 3D electrospun polymer substrates.

- The device keeps track of substrate elongation and forces in real-time as the force to elongation curve determines the substrate stiffness.

- Characterize Polymers mechanical properties, since they are the mechanotransduction scheme for cultured cells.

- Propose a real-time biocompatible cost-effective precise technique that is easy to modify and fabricate as required.

- Explain the principle of operation, related theories, design and fabrication process.

- Calibrate biosensors, mechanically test polymer scaffold substrates and discuss results.

Chapter Two

Methods

2.1 A Description of the Device Function and Design

The real-time method applies measurable uniaxial longitudinal tensile forces and observes the resultant elongation in substrate samples. A mechanical stage displacement (s_2) is used to deliver tensile forces as described in fig.1 and 2. The resultant micro-strain that substrate samples undergo is continuously monitored by using microscopic post-processing digital image correlation setup. The device is also coupled with a laser-based optical lever force sensing scheme.

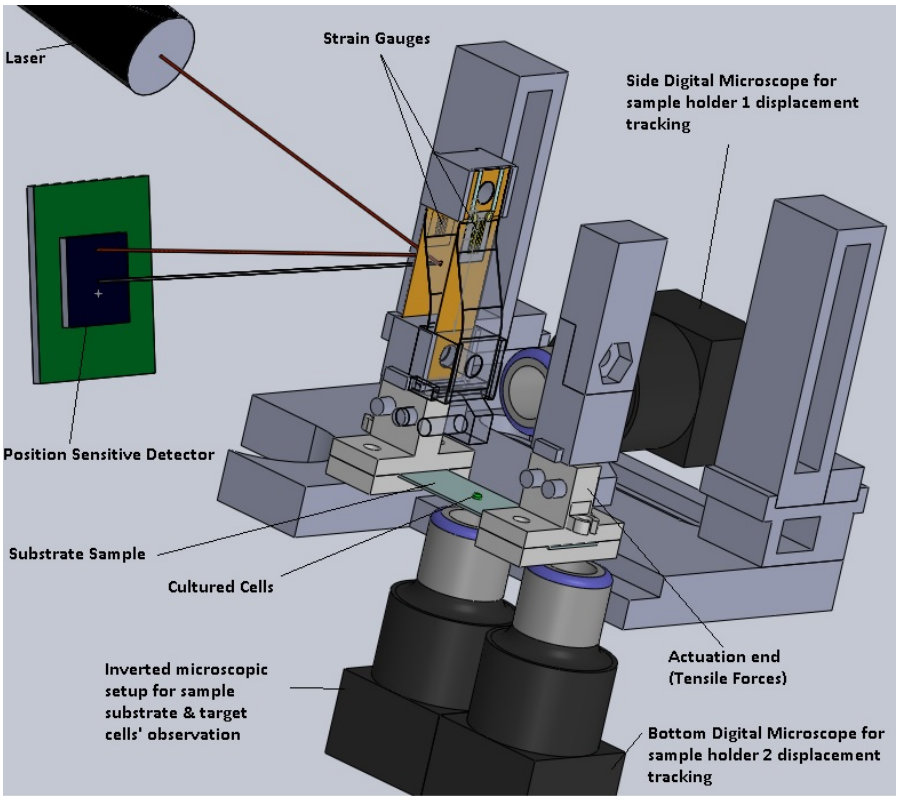

Figure 1: Instrument design isometric view (with section cuts).

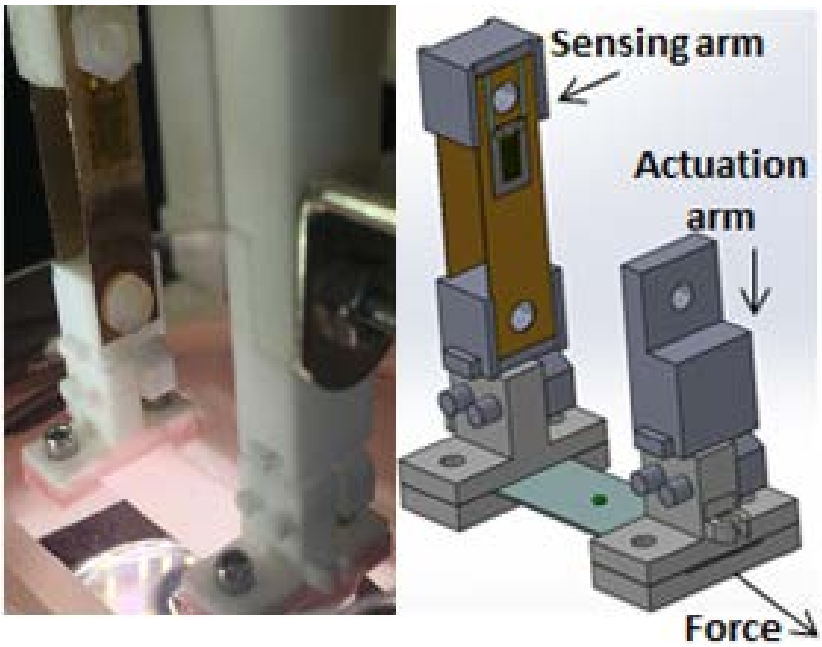

Figure 2: Active arms in the system (left image shows immersed active arms in media)

2.1.1 Principle of Operation

The principle of operation in this design relies mainly on Hookes' law, where tensile forces applied by the stage pulls the substrate sample and stretches it from one end to the +X-axis direction. The other substrate end is attached to an equivalent spring (a parallel leaf spring configuration) that has an elongation s_1 on the same axis of the mechanical stage movement. The equivalent spring is fixed from its other end. The electrospun nanofiber substrate polymers used in this study have an elastic region in the stress-strain curve, and that is the reason behind using such nanofiber substrate polymers as another spring in series connection in this model. Indeed, the substrates' physical dimensions play a significant role in changing the stress-strain relationship. For this reason, the substrate sample dimensions were fixed through this study.

The idea of two series springs that has a stiffness $k_1$and k_2 obeys Hooke's law Eq.6 section 2.3, where both springs carry an elongation $s_1$and ΔL respectively, in the same direction and axis of applied force fig. 2, 3A and 3B.

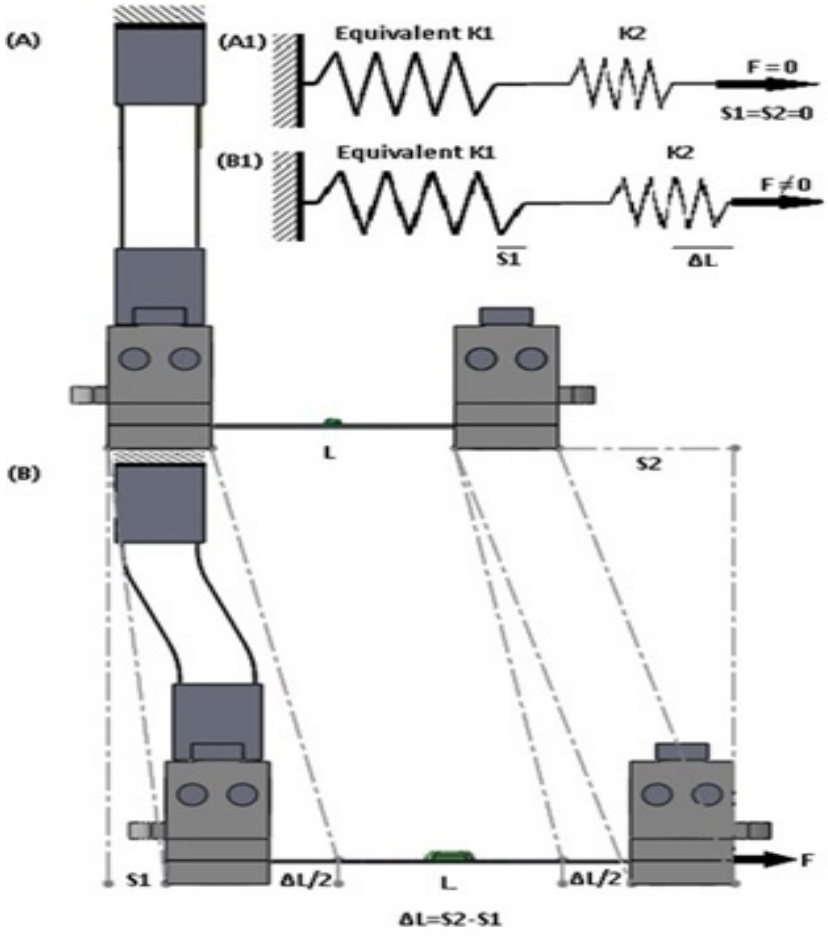

Figure 3: (A) System initial equilibrium state, (B) System deformed by force f, and (A1) represents (A) while (B1) represents (B) in the corresponding spring schematic diagrams.

2.1.2 Design Considerations

The actual structure used to build the first equivalent spring is composed of two parallel leaf springs. This configuration is calculated and considered as one equivalent series spring that has a major component of elongation s_1 on the same X-axis in this model. On the other hand, the motion of the movable part in the parallel spring has a parasitic motion component in the Y-axis as shown in fig.4A and it is a function of $s_1 = s_x$. Moreover, in case the tested specimens were too stiff compared to the equivalent spring, further modification may be required to the spring material or design dimensions. (Equivalent spring stiffness calculation is covered in section 2.3). Adding to the principal of operation regarding design consideration, when a restorative parallel spring configuration (shown in fig. 7 Section 2.4.2) is added in series to the model, it takes the displaced second substrate holder back to its initial position after tensile forces are released. The first equivalent spring brings the first substrate holder to its initial location. When using the schematic diagram shown in fig.3A_1 & 3b_1 to describe the third restorative spring, it gets compressed when other springs in the model get stretched, and vice versa since the force is applied in between. The third restorative spring is not represented in calculation nor hypothesis of stiffness measurement as it is bypassed during substrate stretching stiffness measurements. The material, fabrication, and design of this eight parallel flexures' spring are shown in section 2.4.1.

2.2 Continuous Strain Measurements and Force Correlation

2.2.1 Strain Gauges and Digital Microscopic Setups

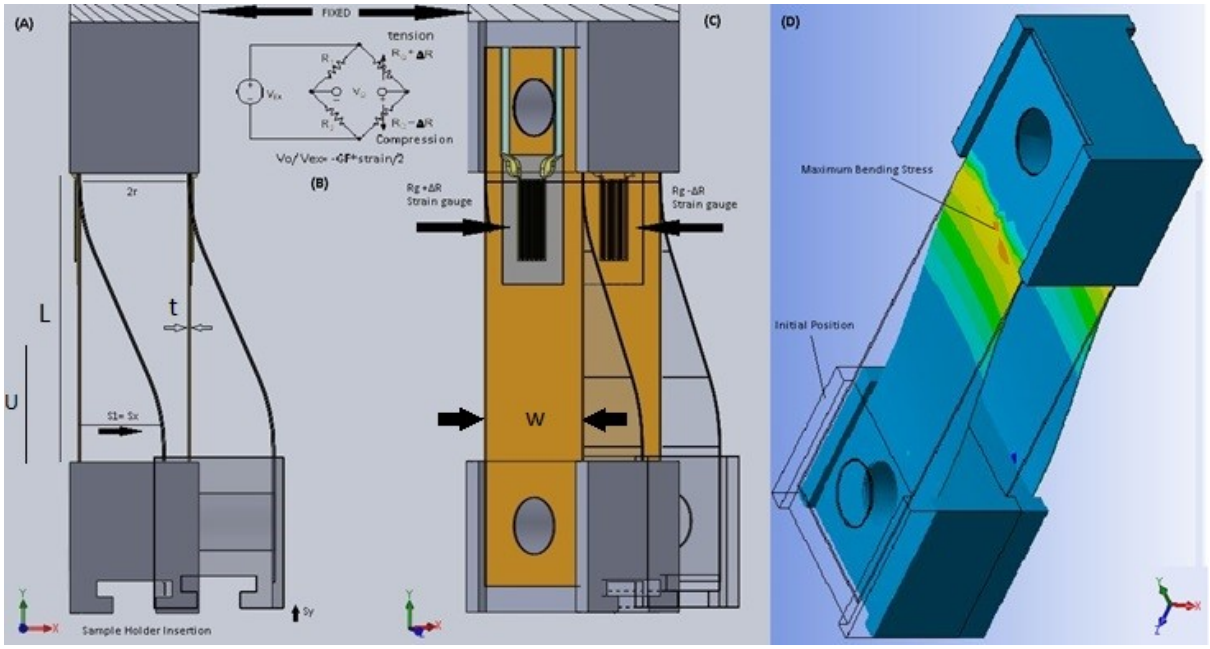

Figure 4: (A) Parallel leaf spring configuration and parameter definition. (B) Wheatstone half bridge representative circuit. (C) Parallel leaf springs showing strain gauges' attachment. (D) Simulation showing the maximum stress points.

Strain gauges (OMEGA, 120.4 ohms ±0.35%, GF=2) in a Wheatstone half bridge arrangement, as shown in fig.2, 4b & 4c, were attached to the parallel leaf springs at the maximum stress points as shown in fig.4D. Based on structural mechanics, as a result of applying force to a parallel spring configuration, leafs bend forming S shape like pattern; the maximum tension and compression occur closest to the fixed support. Based on Hookes' law, the force applied to series springs is equal. Therefore, based on strain gauges and calibration data, we can continuously correlate the equally applied forces f that result in an elongation s_1 and ΔL of both series springs and determine the spring stiffness k_1 then k_2, respectively.

In addition, two microscopic setups track both edges of the substrate holders by digital image correlation shown in fig.1. Images taken using the first digital microscope (side viewing) were scaled using a micrometer ruler, and the edge of the first substrate holder displacement s_1 was observed. The first microscopic setup tracks the equivalent spring elongation s_1. Similarly, displacement of the second edge of the substrate holder s_2 is measured by a second digital microscope (inverted vertical view) and the elongation in the substrate ΔL is then calculated based on the model in fig.3B. By continuously measuring the applied force and resultant elongation we get the stiffness of the target substrate. By knowing the target dimensions, the stress-strain slope (Young's modulus) is calculated based on section 2.3.

2.2.2 Laser-Based Optical Lever Sensing of Spring Bending Forces

The second sensing element forms an optical lever. A fixed incident laser beam (650nm) is directed as tiny spot through a numerical aperture on the polished phosphor bronze spring midpoint. Before bending, the laser incident angle α^{o} with respect to the normal of the spring is reflected back with a reflection angle α^{o} like a mirror. The reflected laser beam have an angle $2\alpha^{o}$ from the fixed incident laser source as shown in fig.5a.

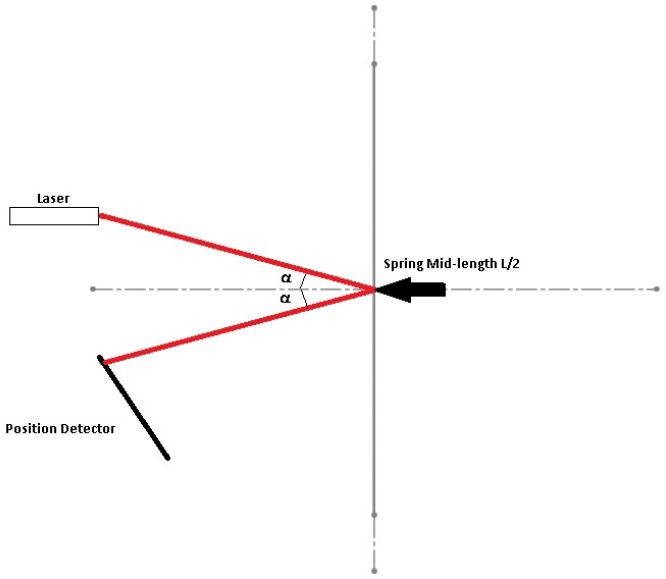

Figure 5: (a) Mirror like reflection with no offset and no tilt angle. (The X-axis is the mid-length of the leaf spring)

The reflected beam is captured on a Position Sensitive Detector (PSD) (Hamamatsu, active sensing area 4mm*4mm), which is located at a fixed distance δ from the reflection point. The PSD detects the reflected laser spot displacement due to mechanical spring deflection when force is applied, and since the parallel spring configuration becomes like an S-shape when forces are applied. The maximum angle of a deflected leaf spring occurs around the midpoint $(L/2)$; which make the laser based optical lever so sensitive to (μN) applied forces. When spring bending occurs, an offset from the original y-axis takes place and a tilt angle. In fig.5b, we consider the offset:

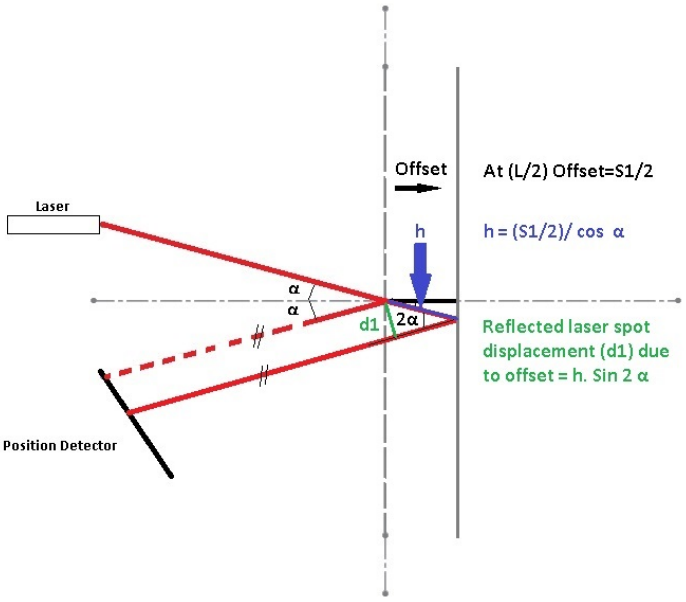

Figure 5: (b) Mirror like reflection with offset and no tilt angle Øº, (dashed red line is the initially reflected spot when F=0, solid red line is displaced on PSD by d1).

The parallel spring elongates by $s_1$at length L_1 when applied force $F > 0$, then the displacement d_1 at the mid length $L/2$ is proportional to the applied force f, where $d1 = (s_1/2)/cos\ \alpha$. Figure.5c explains the tilt angle $\emptyset^{o}$ and the offset.

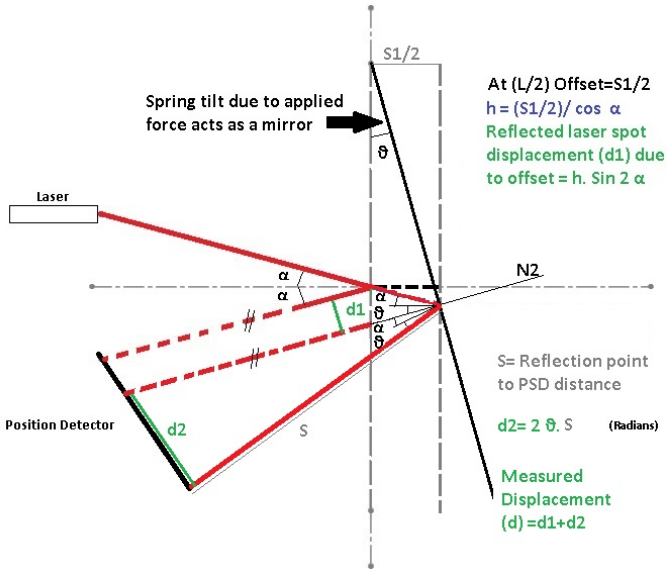

Figure 5: (c) Mirror like reflection with offset and tilt angle Øº, (dashed red line is the previously reflected laser spot [fig 5, a &b], Solid red line is displaced by d1+d2).

When the spring bends by an angle $\emptyset^{o}$ due to an applied force f, the normal of the spring tilts by an angle $\emptyset^{o}$ additional to the offset in position. Consequently, the reflected laser angle becomes $2\alpha^{o} + 2\emptyset^{o}$ with respect to the fixed laser source. Then, tilt and offset considerations are shown in fig. 5C; where the difference between the final reflected beam angle $2\alpha^{o} + 2\emptyset^{o}$ and the initially reflected beam angle $2\alpha^{o}$ both from the fixed incident laser beam is $2\emptyset^{o}$, which is a component of the total displacement of the reflected laser spot d detected on the PSD at a fixed distance δ. Due to bending, $d2 = 2\emptyset^{o} * \delta$ (radians), meaning that the displacement of the reflected laser spot d_2 is also proportional to the applied force. For better measurements, the PSD active sensing length d, the PSD tilt angle, and its distance δ from the reflecting point is considered according to the figures 5a, b & c.

Then, we correlated the reflected laser spot displacement with the applied forces on the leaf spring 1; the laser based optical lever setup was also used to monitor stretching and contraction of the substrates even in between applied forces. The laser sensing configuration was also used as an alert when deflection limits were reached or exceeded; this way we confirm the results of the bridge and continuously monitor any small forces causing spring bending.

2.3 Equations Used to Characterize Materials Mechanical Properties

***Stress*:** $$\sigma = \frac{f}{A} \quad (1)$$

is the force (f) applied to a cross section Area (A)

***Cross Section Area*:** $$A = wt \quad , \quad (2)$$

The width is (w), and (t) is the thickness of the substrate sample.

***Strain*:** $$\varepsilon = \frac{\Delta L}{L} \quad (3)$$

The strain **Ɛ** is the ratio of the extended length (ΔL) to the original length (L).

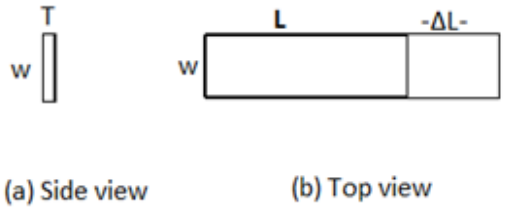

Figure 6: Defining dimensional parameters. (a) Target side view. (b) Top view of the elongated specimen.

***Young's Modulus*:** $$E_2 = \frac{\sigma}{\varepsilon} \quad (4)$$

Which is the tensile modulus referred to as stress (σ) to strain (Ɛ) ratio, where the original length (L) and width (w) of the polymer samples are fixed before mechanical stimulation. Young's modulus (E_2) will rely on the thickness (t) of the polymer sample undergoing tensile forces (f) to show an elongation in length (ΔL). The area (A) and length (L) are fixed in this study.

The hypothesis behind this device measurement method mainly relies on Hooke's law. Even though the used springs are not actually in series, they act as two equivalent springs connected in series, one of known stiffness and the other is the tested substrate sample. The equivalent spring has one end fixed, and the other end has a pulling force that elongates both substrate and first equivalent spring by (ΔL) and (S_1) respectively when actuated in +X-axis.

$\boldsymbol{Hooke's\ Law}$: $$\boldsymbol{f = -ks} \quad \textbf{(5)}$$

Where (K) is the stiffness, or spring constant and (S) is the elongation of the spring, the $(-ve)$ sign indicates that it is a restorative force.Similarly, when using the first equivalent spring (1) and the polymer substrate as spring 2 in a series configuration the relationship will be as follows:

$$\boldsymbol{f = -k_1 \times s_1 = -k_2 \times \Delta L} \quad \textbf{(6)}$$

The first equivalent spring stiffness k1 is the stiffness of two parallel S-shaped leaf configuration. The X-axial elongation (s_1) is measured using a first digital microscope while the stiffness of the substrate sample (K_2) will resist the force (f) that is stretching the sample by the same amount in both directions. This result in an elongation s_2 that is monitored using a second digital microscopic setup on the other polymer holder where: $(\boldsymbol{\Delta L}\ substrate\ elongation = s_2 - s_1)$ As shown in fig.3b.

From Hooke's law in Eq.5, the stiffness (K2) is related to (E2) Young's modulus in Eq.4 by the following relationship:

$$\boldsymbol{E_2 = \frac{k_2 * L_2}{A_2}} \quad \textbf{(7)}$$

For parallel leaf spring stiffness measurement, calibration of the equivalent spring 1 relies on Eq.5 using known accurate loads and measured elongation (calibration data in section 2.5.2).

Moreover, Young's modulus of the combined equivalent spring (E_1) is based on the parameter definition shown in fig. 4A, the following equations were considered:

$$\boldsymbol{I_1 = \frac{w_1\ t_1^3}{12}} \quad \textbf{(8)}$$

$$\boldsymbol{k_{1_x} = \frac{24\ E_1\ I_1}{L_1^3}} \quad \textbf{(9)}$$

$$\boldsymbol{k_{1_y} = \frac{2\ E_1\ A_1}{L_1} \quad only\ if\ s_1 = 0\ ;} \qquad \boldsymbol{k_{1_y} = \frac{1400\ E_1\ A_1\ I_1}{L\ (700\ I_1 + A_1\ s_1^2)} \quad for\ s_1 \neq 0} \quad \textbf{(10)}$$

$$\boldsymbol{k_{1_z} = \frac{2\ E_1\ t_1\ w_1^3}{L_1^3}} \quad \textbf{(11)}$$

$$\boldsymbol{s_{1_x} = \frac{\sigma\ L_1^2}{3\ E_1 t_1}} \quad \textbf{(12)}$$

$$\boldsymbol{s_{1_y} = \frac{0.6\ s_{1x}^2}{L_1}} \quad \textbf{(13)}$$

Where (I) is the moment of area of the S-shaped spring deformation. In this study, the series spring configuration shown in image 3B will only consider k_{1_x} and s_{1_x} as k_1 and $s_1$in all calculations. As the parasitic motion s_{1_y} is relatively negligible. The parasitic motion is measured by the first microscopic vertical setup, and those displacements are considered during cell monitoring and focus compensation.

If we look at one spring from the parallel leaf configuration, we can calculate its deflection (D) at a specified length (U) by following the equation:

$$\boldsymbol{D = f * U^2 * \frac{(3L_1 - 2U)}{12\ E_1 I_1}} \quad \textbf{(14)}$$

It is necessary to know the best spot for the laser reflection on the leaf spring (mentioned in section 2.2.2) as the reflection should take place at the maximum tilt angle. Based on calculation eq.14 and simulation fig.6, the maximum angle is around length $(L/2)$ of the spring.

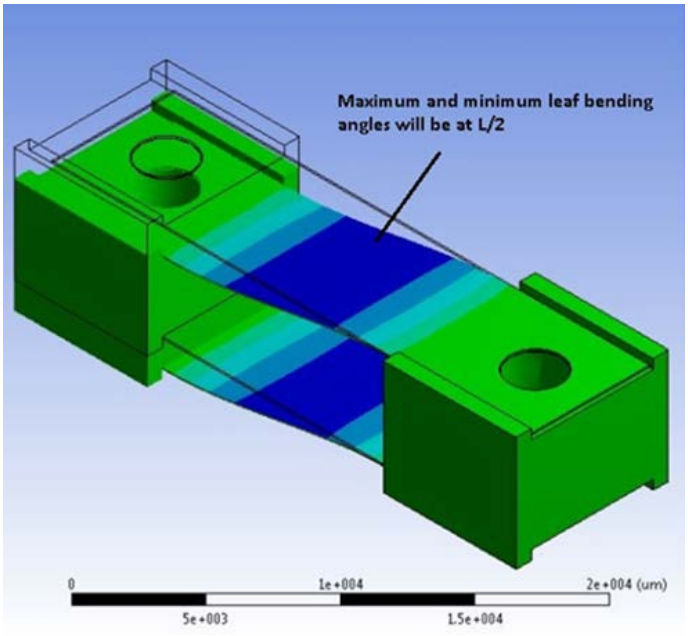

Figure 6: Maximum tilt angle area simulation

For calibration, Newton's second law is used with respect to gravity as follows:

$$\boldsymbol{f = mg \cdot \sin \theta} \qquad \textbf{(15)}$$

Where (g) is the gravity acceleration vector (9.8066m/s²), (m) is the mass, and (Θ^{o}) is the angle if there is a tilt or angular configuration.

2.4 Fabrication and Materials

2.4.1 3D Printed Assemblies and Subassemblies

In the proposed device, the parts were designed using CAD software (Solidworks), fine polyamide (PA 2200) is the 3D printed material. It constructs the 3D assemblies which represent the main chunk of the apparatus shown in figure.7. These images do not include the two parallel leaf springs as their microfabrication and material are different (explained in section 2.4.2).

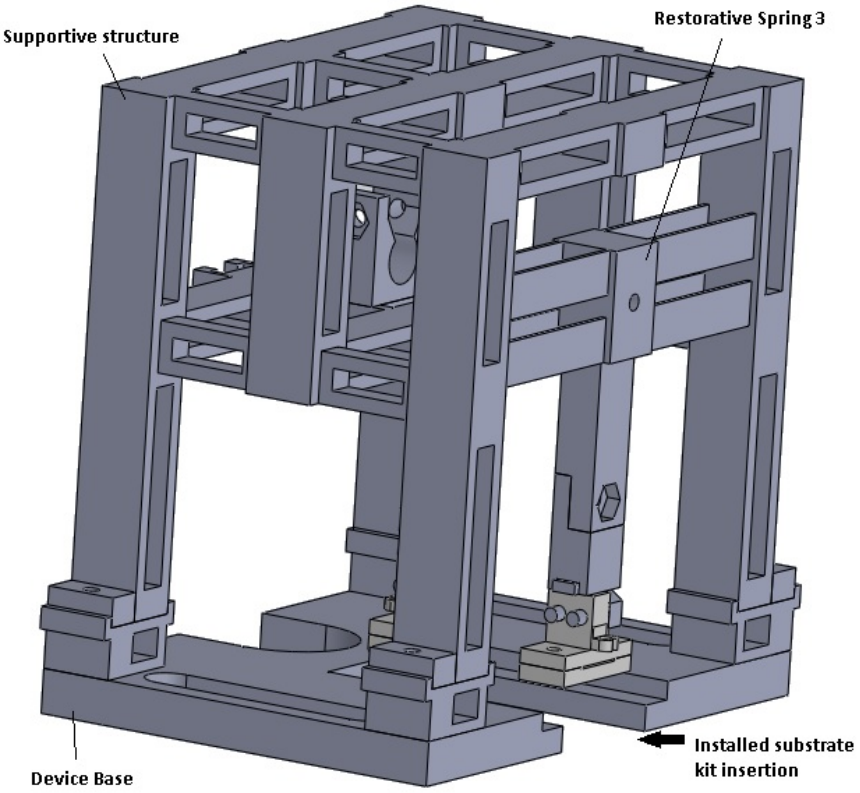

Figure 7: Polyamide 3D printed assembly

The fine polyamide (PA 2200) chemical composition is known as (Polylaurinlactam (polyamide 12)). The solid polymer has mechanical characteristics as follows; a tensile modulus of 1700 Mpa, a tensile strength of 48 Mpa, and a flexural modulus of 1500 Mpa acquired from the material data sheet (EOS GmbH - Electro-Optical Systems through Shapeways). In regards to

biocompatibility, the solid polymer is water-insoluble, which, under cell culturing environmental conditions, is not expected to have a harmful effect on microorganisms.

The substrate installation kit shown in fig.8 was also 3D printed from the same polymer (PA 2200). The kit keeps a fixed distance (length of tested substrates L_2) in between the holders until it is attached to the stretching/sensing unit and ready for testing.

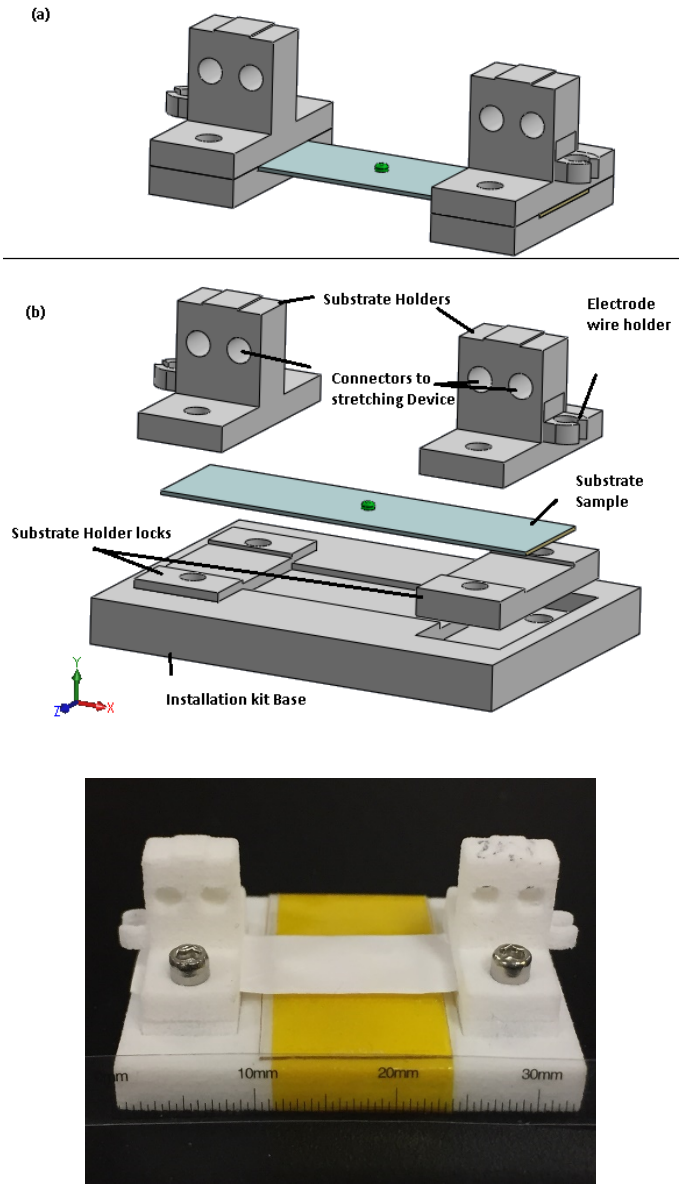

Figure 8: (a) Substrate holders attached to polymer substrate and ready for testing. (b) Detached individual parts of the installation kit (c) actual polymer installation kit.

When the substrate holders lock the electrospun nanofiber polymer sheet on the installation kit base, it is slid in an insertion under the stretching/sensing arms (shown in fig.2, 7, 8) and slowly attached to arms' cylindrical connectors through the connector holes. Then, just before mechanical stretching, the installation kit base is slid down and removed.

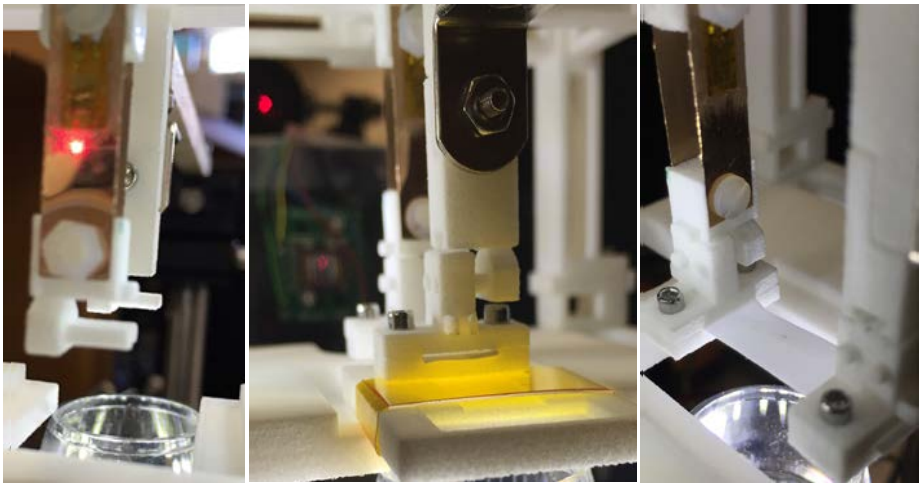

Figure 8: polymer Installation kit attachment to active arms (d) before installation (e) during installation (image from opposite side), (f) after installation to active arms

2.4.2 Leaf Springs Fabrication

The parallel leaf springs were fabricated from phosphor bronze sheets (100µm) thick (25mm) total length while the active bending length is (L_1=13.4mm) as illustrated in fig.4a & c, and calculations were considered accordingly. The metal sheet was wiped and cleaned softly using DI water and a sponge. Then, negative photoresistive films were used to make a sandwich above and below the metal layer as shown in fig.9a. At the side of photoresist attachment, the protective layer has to be removed; DI water is used in between for better alignment. After film attachment, the sandwich of photoresist over the metal sheet was heated using a roller laminator for better attachment and to avoid bubbles in between caused by DI water.

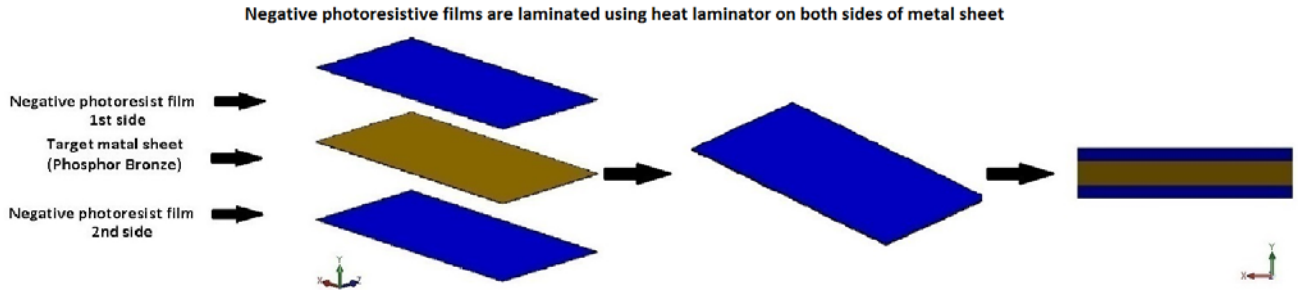

Figure 9: (a) Metal sheet-photoresist sandwich lamination & their side view

Photomasks were aligned on both sides of the photoresist sandwiching the metal for UV photolithography patterning as shown in fig.9b.

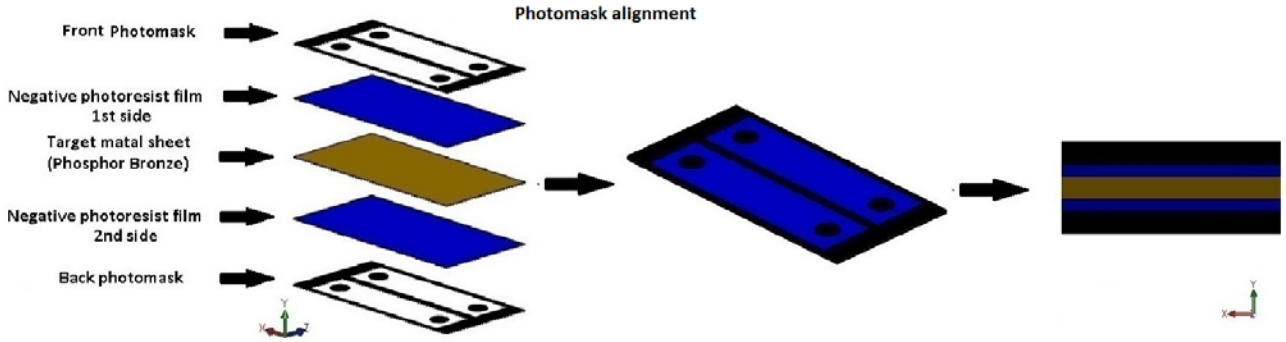

Figure9: (b) Photomasks alignment & their side view

The patterning used (15 sec UV exposure) through designed masks to pattern negative photoresistive films on the phosphor bronze sheet, then the photomask was removed, and the photoresistive protective layer was also removed using an adhesive tape as shown in fig.9c.

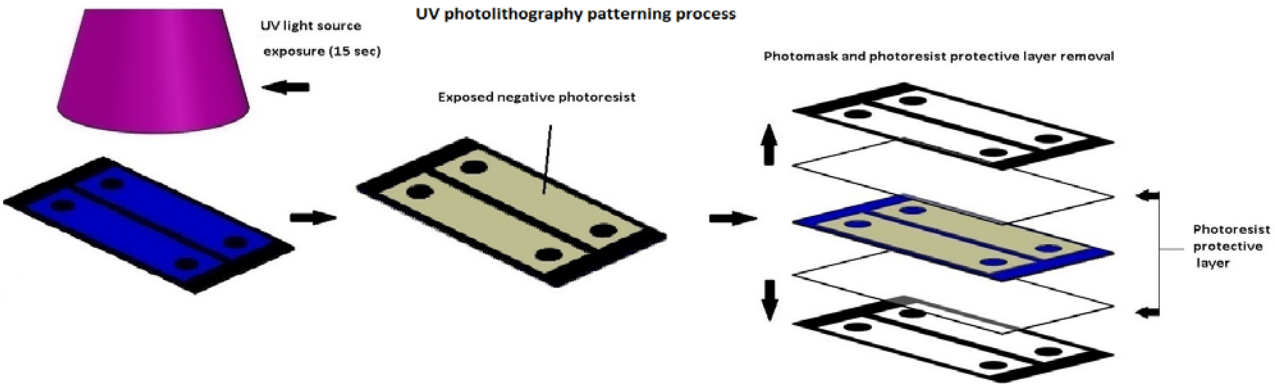

Figure 9: (c) Ultraviolet photolithography Patterning

Then, the photoresistive film's sacrificial layer is removed using a (Micro-Mark, Pro-Etch) developer (30 sec), which contains sodium hydroxide. Next, metal etching (≅ 17-20 min) takes place to remove unprotected and unwanted metal features using a metal etching solution, which contains ferric chloride $FeCl_3$, obtained from (Micro-Mark, Pro-Etch). After metal etching, the microfabrication process requires the removal of the exposed photoresist (protective layer), Acetone was used to rub the exposed photoresist away as shown in fig.9d.

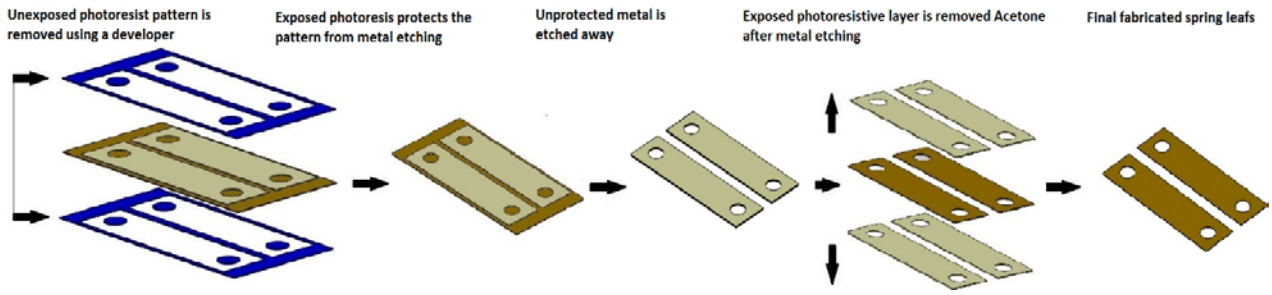

Figure 9: (d) Photoresist Development, metal etching, and final product

After fabrication, to use the phosphor bronze leaf spring as a mirror for laser beam reflection, the spring was polished using (Metal polish cream, Bluemajic.Inc) except for the strain gauge attachment area. In fact, surfaces of leafs where the gauges were attached were softly scratched. The reason was to make them rough for easier strain gauges' attachment when a distributed drop of super glue is used. An image of the fabricated leafs is shown in fig.10a while fig.10b shows the polished/filed spring leafs (ready for strain gauges attachment).

Figure 10: (a) Fabricated leafs (b) Half polished and scratched springs, the left leaf is reflecting room light

Springs and the substrate samples are not in direct contact, nor cell culturing media to ensure proper experimental biocompatibility even in compact cell culture incubators or Petri dishes used for cell culturing.

2.4.3 Electrospinning nanofiber polymer substrates

The polymer solutions were kindly provided by the Institute of regenerative tissue engineering at University of Connecticut Health Center UCHC. The solutions used in electrospinning include Poly-ε-caprolactone (PCL) and Cellulose Acetate (CA). The mixtures had the following concentrations, (PCL)100:0, and (PCL: CA) 95:5, 90:10, 80:20 in 12.5% solutions. The electrospinning fabrication process of polymer sheets is illustrated in fig.11a while the actual image of the setup is shown in fig.11b.

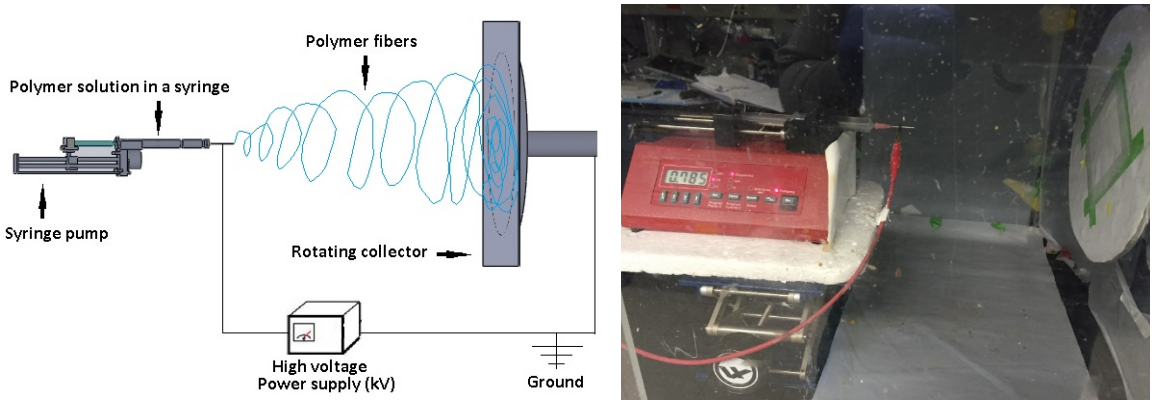

Figure 11: (a) Electrospinning fabrication principle, (b) Electrospinning fabrication setup

All four compositions were electrospun on aluminum foil sheet targets (3 in*3 in) attached to a spinning grounded collector; the distance between the capillary (Taylor cone) and the collector was 20 cm. An electric potential of 14 kV was applied to draw charged threads of polymer solutions' fiber diameters in nanoscale on the aluminum sheet target. A syringe pump was used to flow the four solutions at a rate of 2 ml/hr for 1hr and 14 minutes. In other words, the four resulting nanofiber polymer substrates should have roughly similar thickness.

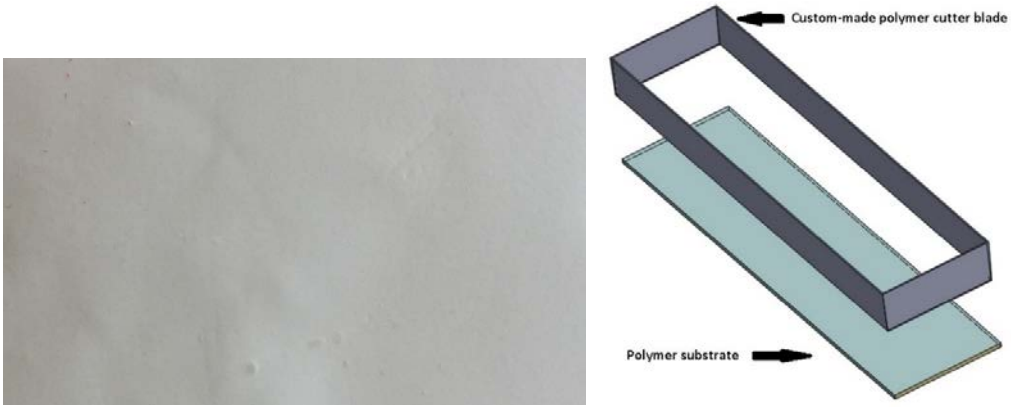

Figure 12: (a) shows a zoomed view of the polymer substrate surface (b) Custom-made polymer substrate cutter blade

After polymer sheets were electrospun as shown in fig.12a, the length and width of substrate samples were fixed using a custom-built polymer cutter blade fig.12b, which was designed to cut specimens to fit the installation kit dimensions accurately as shown in fig.8.

Figure 13: tested specimens in petri dish, a specimen ready for installation (middle) and detached polymer installation kit

The polymer substrates' thickness was measured using a micrometer and for some reason, the PCL: CA 90:10 was almost half thickness of others as shown in table 1:

Dimensions	**PCL 100**	**PCL:CA 95:5**	**PCL:CA 90:10**	**PCL:CA 80:20**
$L_2\ (mm)$	16.5	16.5	16.5	16.5
$w_2(mm)$	8	8	8	8
$t_2\ (\mu m)$	110-120	110-120	55-65	100-110

Table 1: Polymer substrate samples' dimensions mechanically tested

2.5 Calibration Method

The actual elastic modulus and stiffness of the equivalent spring in the axis of interest (x) differs slightly than what was declared in material data sheet as manufacturing and fabrication tolerances affect the actual mechanical properties of the metal layers used in the sensing unit and slight variations may affect the calibration relationship, and measurements. For those reasons, it is required for precise sensing of the applied forces to calibrate the sensor correctly and determine the equivalent spring exact stiffness to measure accurate data.

Before the device was tilted to any angle, the bridge was balanced to zero. The device is then flipped to the side, where calibration data starts from the own spring mass (m_0), the loading basket (m), and then the added accurate loads (m_n). The calibration used Hooke's law Eq.5 and Newtons second law from Eq.15. The force to elongation slope of the spring in the x-axis represents the equivalent spring stiffness k_1 performed as shown in fig.14a & b.

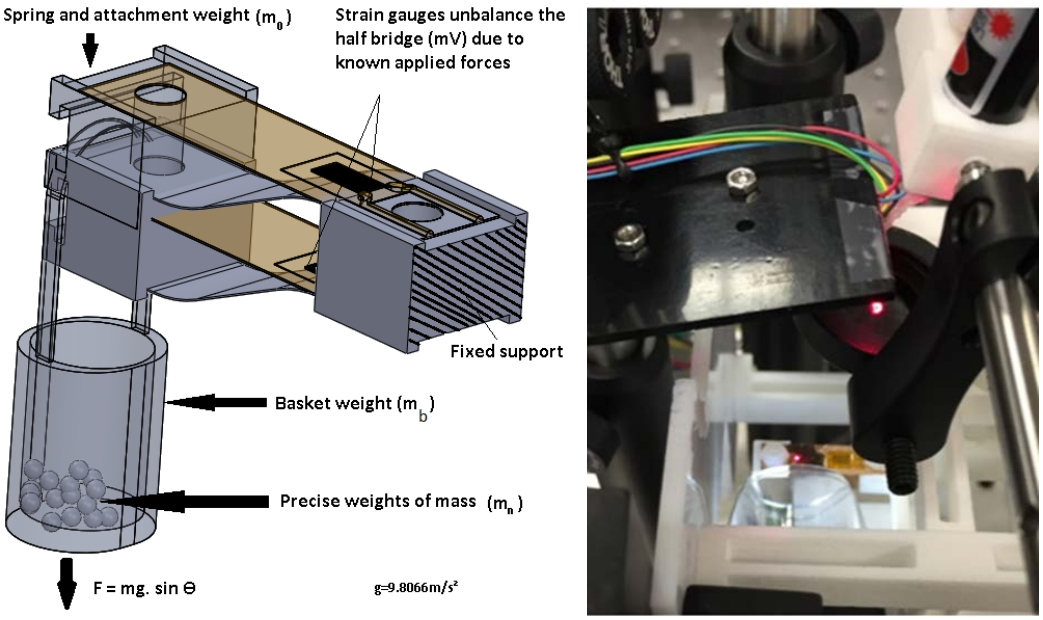

Figure 14: Calibration method (force towards gravity) (a) illustration of calibration, (b) actual flipped sensors calibration

Chapter Three

Results

3.1 Equivalent Spring stiffness k_1, Young's Modulus E_1, and Sensors' Calibration Relationships

The force to elongation slope represents the stiffness curve of the spring as explained in section 2.5. The equivalent spring stiffness (k_1) was measured (0.53 N/mm), and Young's Modulus (E_1) was calculated based on Eq.8 (99.62 Gpa=99628.36643 N/mm²), which falls in the same material properties range in literature (90-110 Gpa). From calibration, the force, elongation, strain gauges bridge, and PSD were correlated as shown below in chart.1:

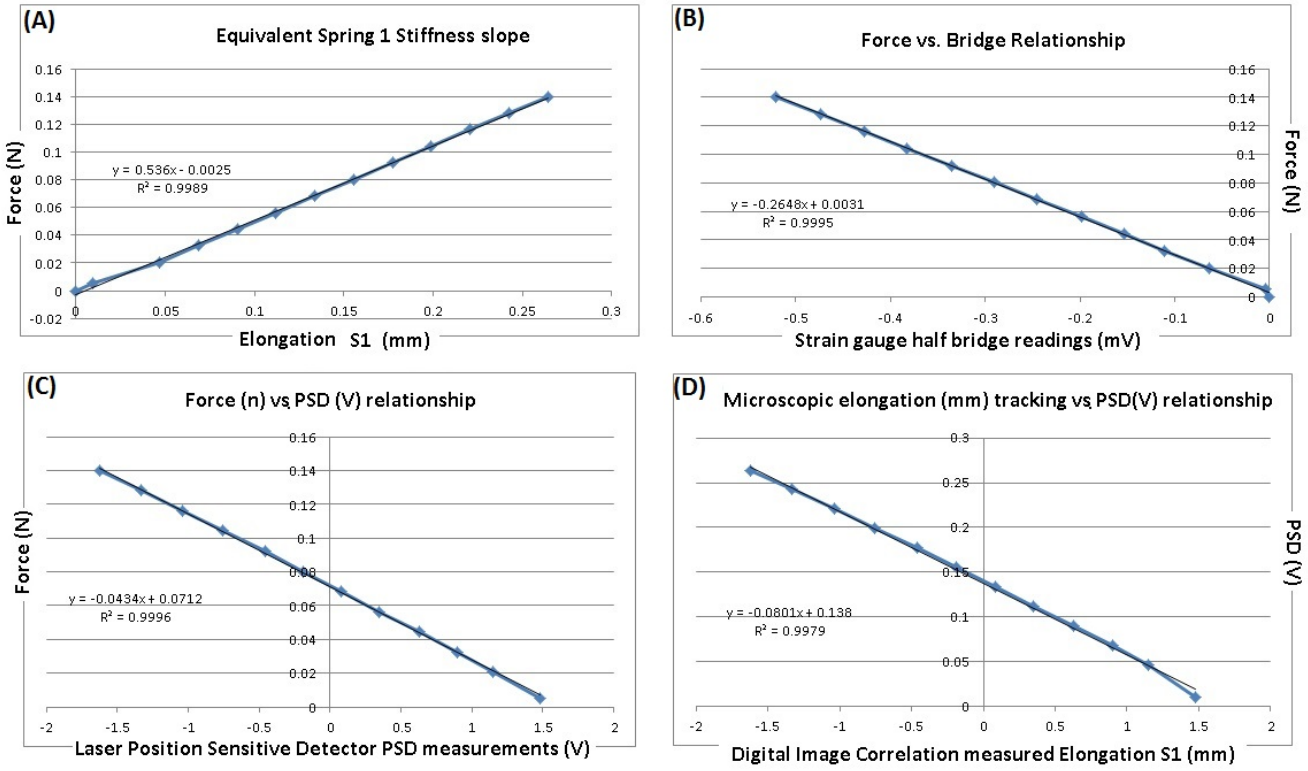

Chart1: Spring 1 calibration (A) Force-elongation (stiffness) curve (B) Force-bridge relationship (C) Force-PSD relationship (D) elongation-PSD

3.2 Nanofiber Polymer Substrates' Measured Mechanical Properties

Mechanical properties characterization of substrate polymers is important since polymer substrates are the mechanical transduction scheme to cultured cells in this system. Poly-ε-caprolactone (PCL) and Cellulose Acetate (CA) nanofibers of different solution composition were electrospun and mechanically tested.

The stress to strain slopes shown in chart 2 (a-d) represent the elastic (Young's) modulus for the four different compositions of PCL & PCL: CA. (measured by our device).

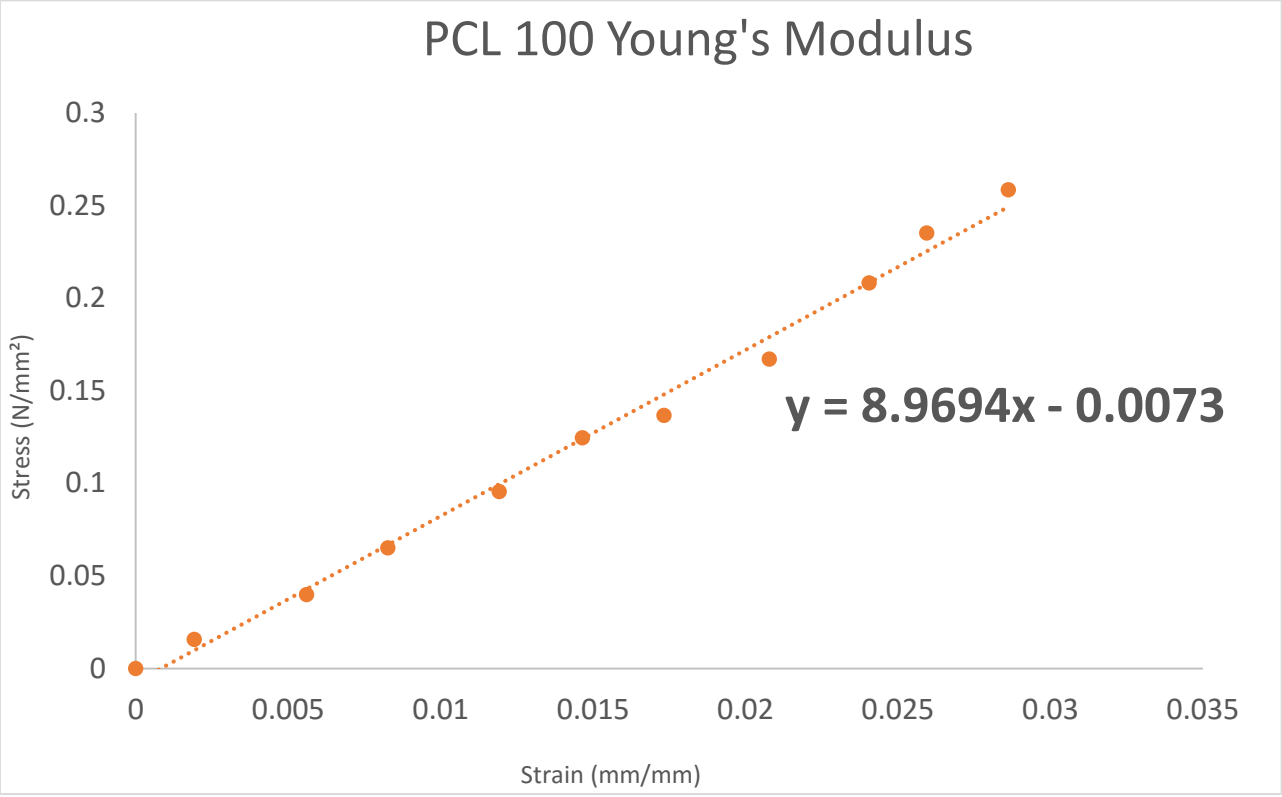

Chart 2: (a) PCL 100 Young's modulus

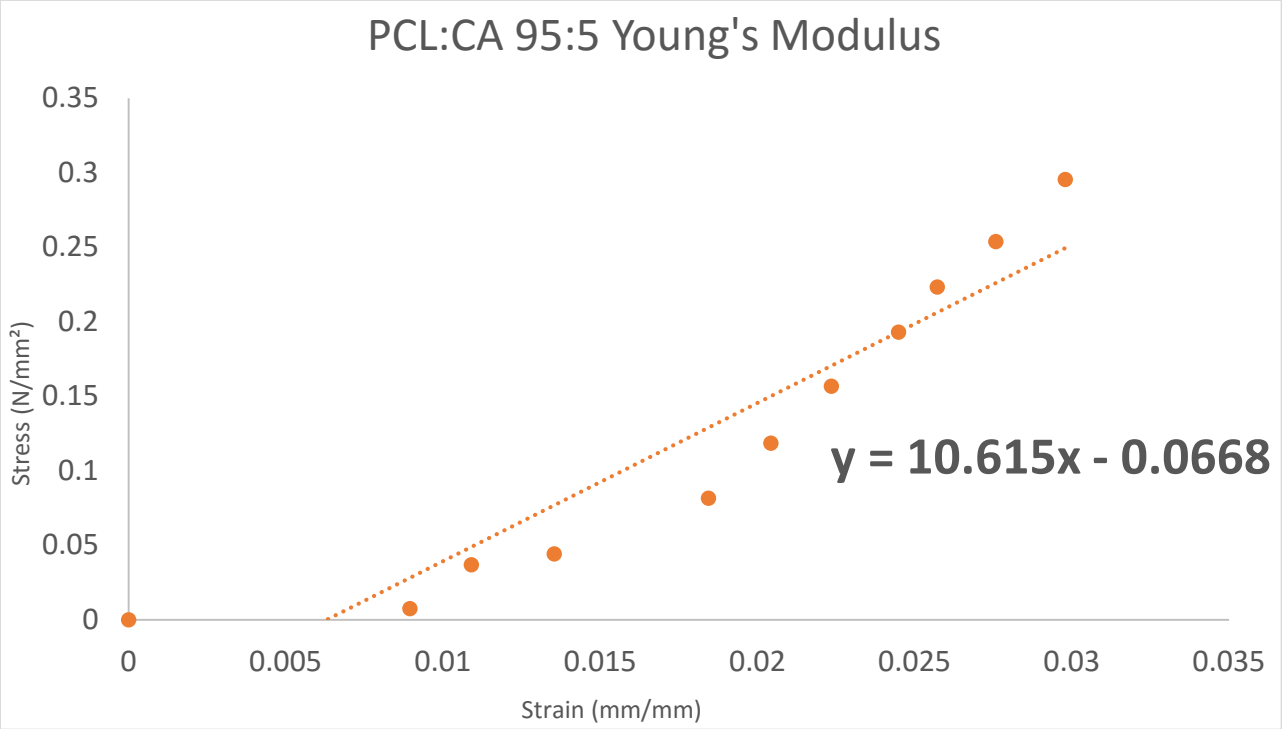

Chart 2: (b) PCL:CA 95:5 Young's modulus

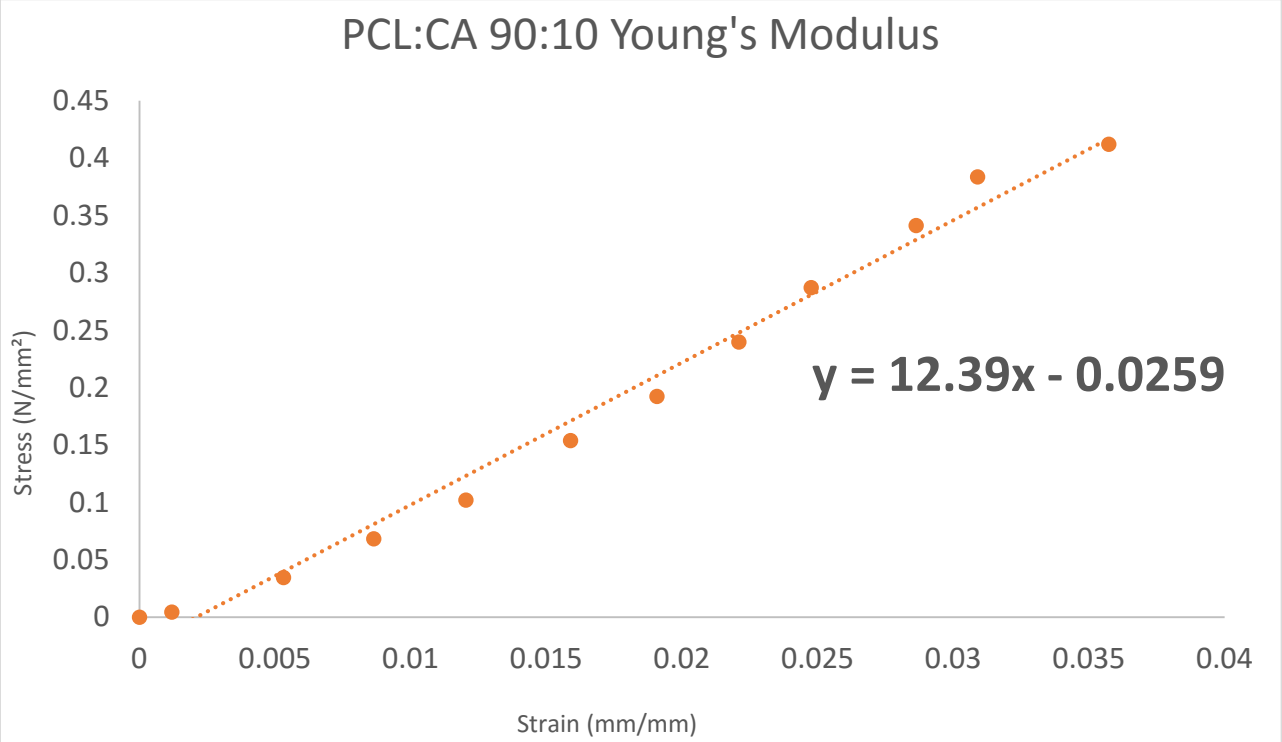

Chart 2: (c) PCL:CA 90:10 Young's modulus

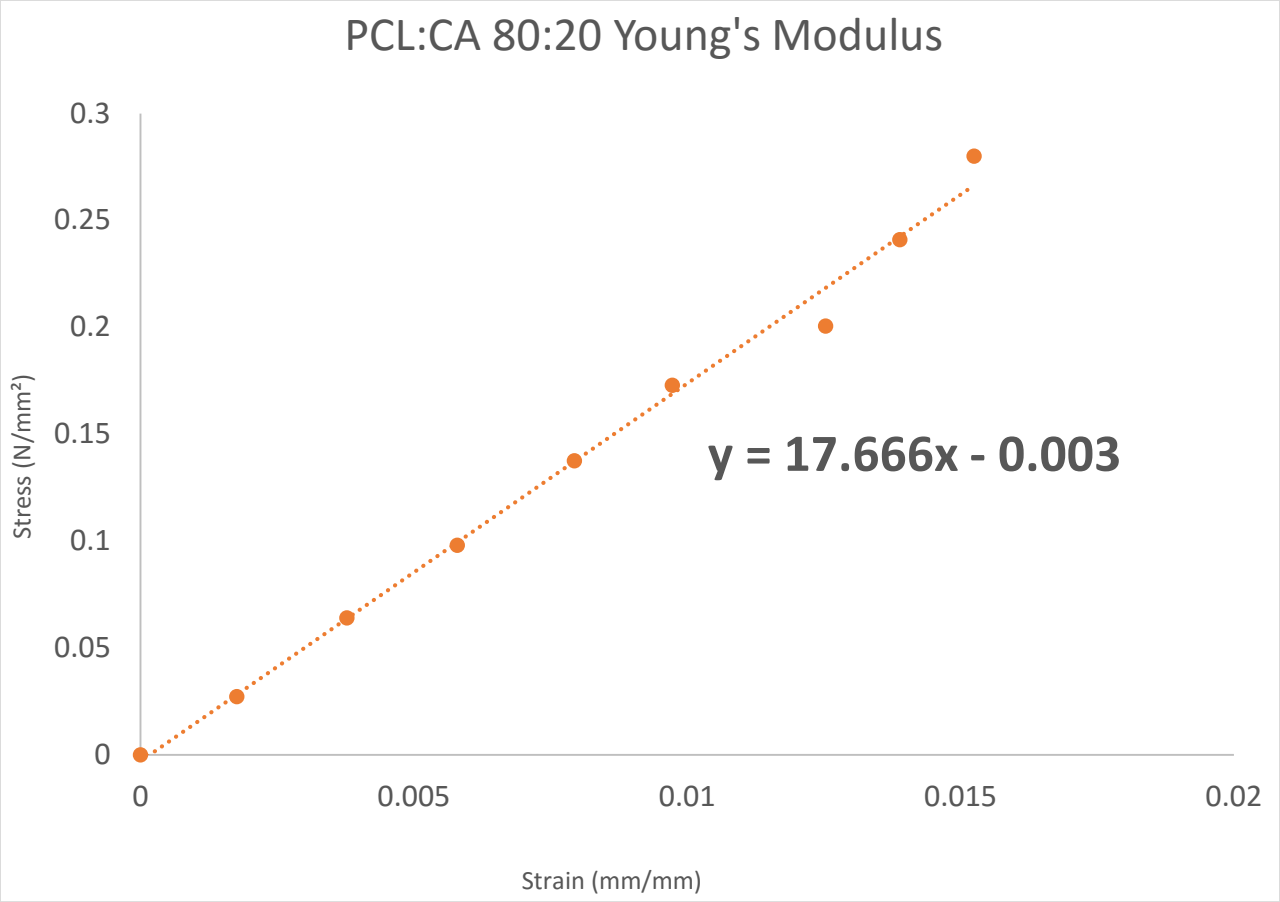

Chart 2: (d) PCL:CA 80:20 Young's modulus

Chart 2 (a-d) show our device mechanical test results, as shown, the elastic modulus slopes are based on a relatively small range of stress and strain.

We mechanically tested identical dimensions (table 1) of the same electrospun sheets (four different polymer compositions) with (Instron 5544) as well. Chart 3 (a-d) show the stiffness average of 3 samples measured by Instron (in orange) and their standard deviation shown as error bars (in black) compared to the stiffness measured by our device (in blue). The tested specimens were prepared similarly in terms of culturing time and media, but during Instron tests, the specimens were taken out of the media and then mechanically tested. The following curves are normalized to fit the same elongations measured by our system.

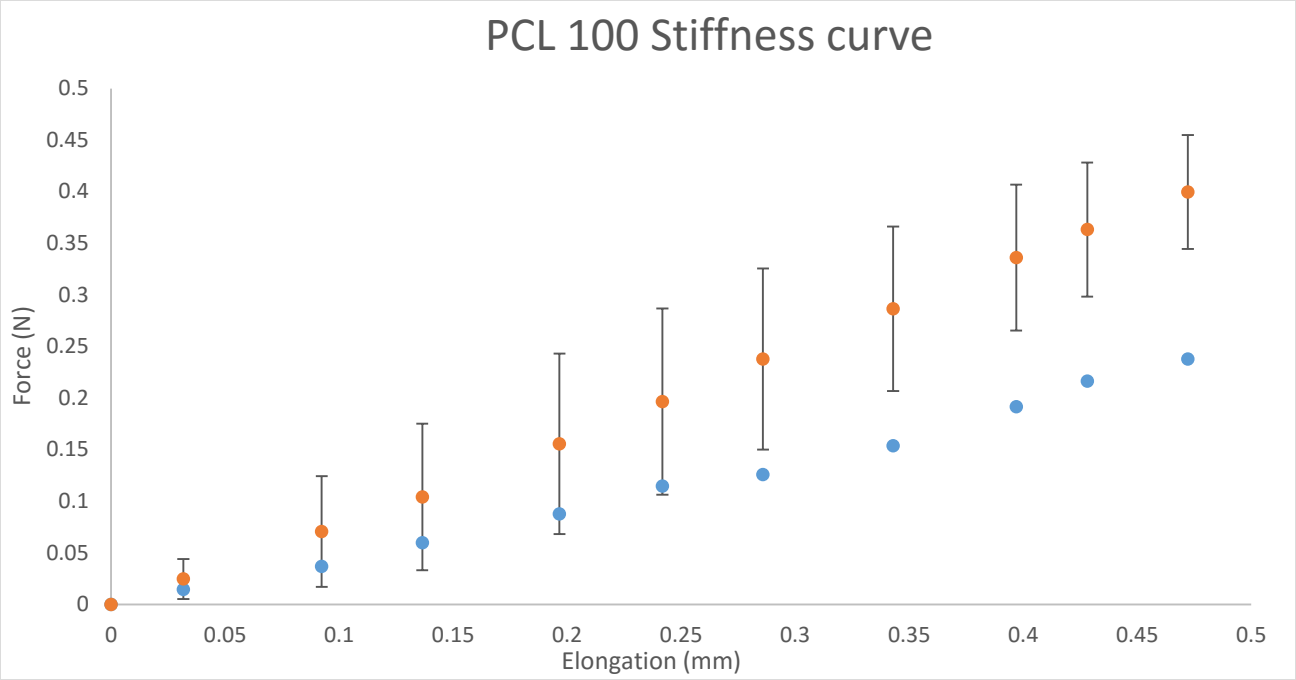

Chart 3: (a) PCL 100 Stiffness test results (Instron results: 3 samples average in orange and their deviation in black bars), (our device results: in blue).

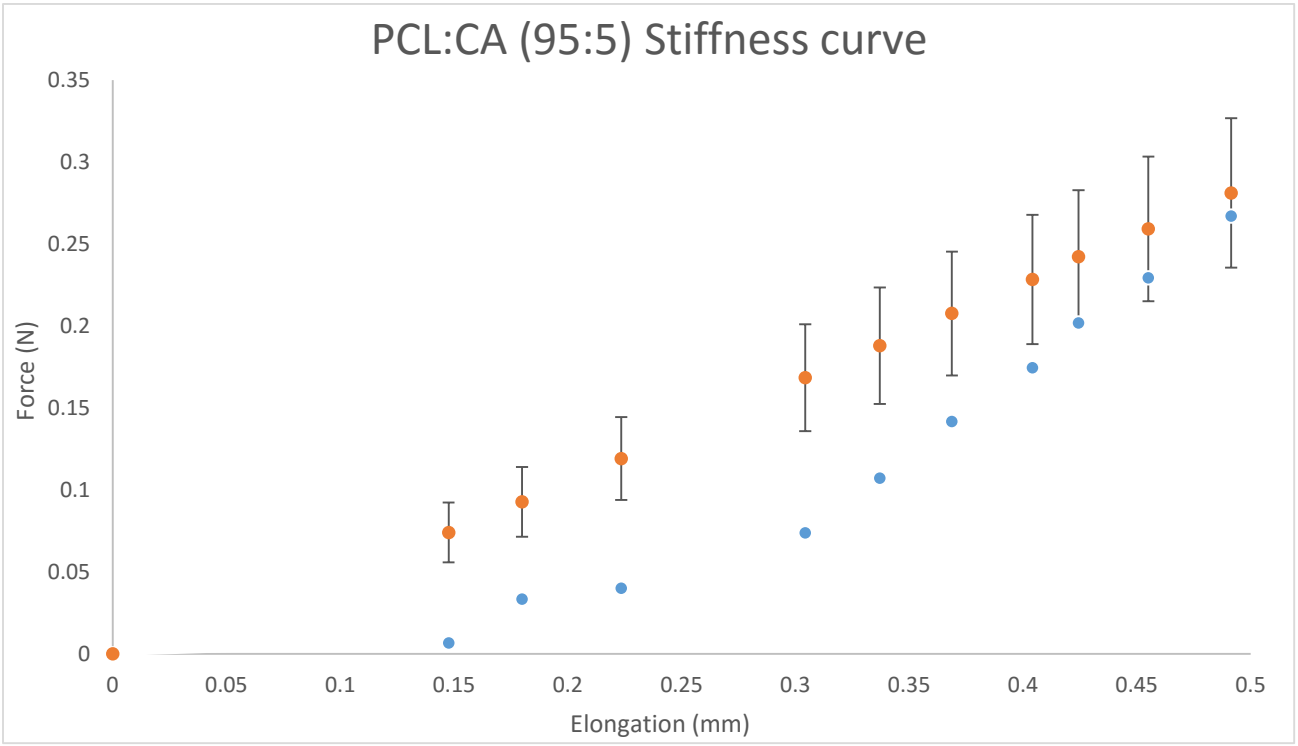

Chart 3: (b) PCL:CA 95:5 Stiffness test results (Instron results: 3 samples average in orange and their deviation in black bars), (our device results: in blue).

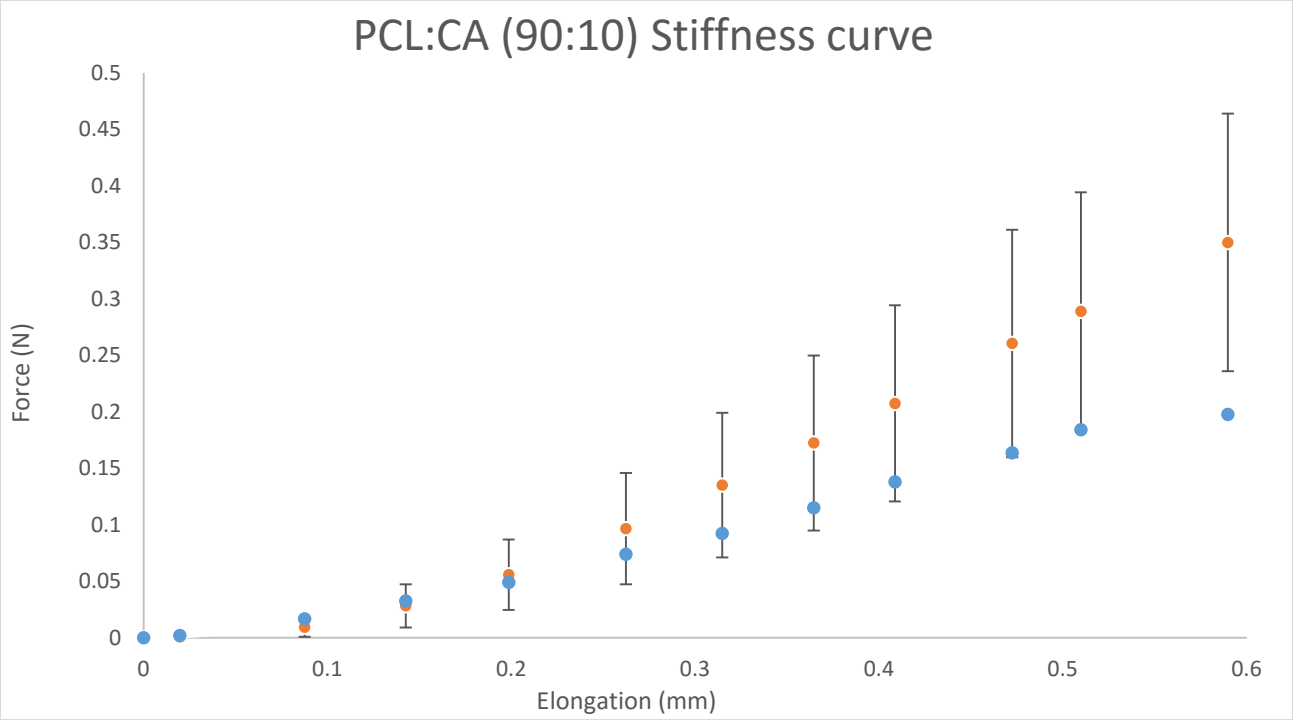

Chart 3: (c) PCL:CA 90:10 Stiffness test results (Instron results: 3 samples average in orange and their deviation in black bars), (our device results: in blue)

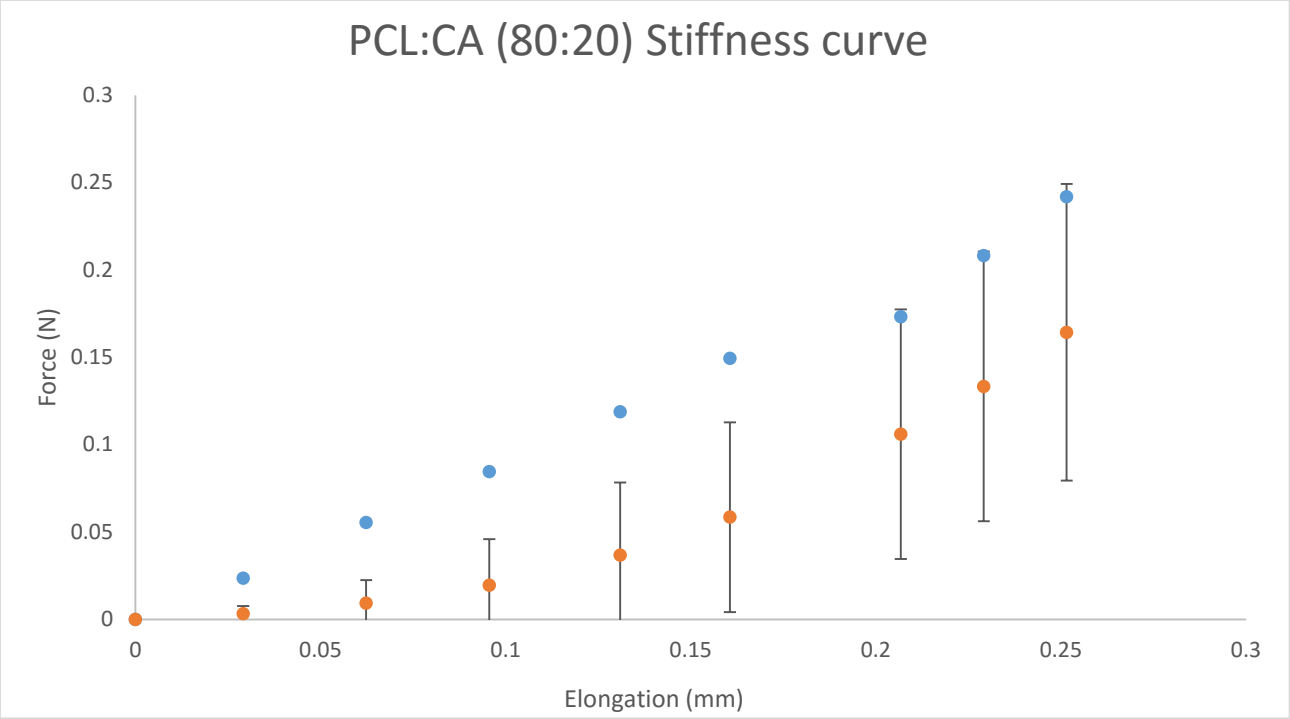

Chart 3: (d) PCL:CA 80:20 Stiffness test results (Instron results: 3 samples average in orange and their deviation in black bars), (our device results: in blue)

Chapter Four

Conclusion

4.1 Sensors Calibration Discussion

- The calibration data shows a linear fit using precise weights with consideration to gravity.
- The device has a range of operation before reaching the spring deformation limit, the range of applied forces will depend on the design, dimensions and materials used.
- The stiffness of spring k_1 (0.53N/mm) has to be comparable to the substrates stiffness k_2, though it is preferred to have a higher stiffness to avoid deformation in case larger forces were used.

4.2 Polymer Testing Discussion

4.2.1 Our Device Results

PCL (100)	PCL: CA (95:5)	PCL: CA (90:10)	PCL: CA (80:20)
8.96 N/mm²	**10.61 N/mm²**	**12.39 N/mm²**	**17.66/mm²**

Table 2: Elastic moduli of tested polymers of different composition

Even though the thickness of PCL: CA 90:10 was around half of others, Young's modulus Eq.4 & 7 considers the dimensions. The mechanically test results match (45) in terms of adding CA% in the composition makes the substrate polymers stiffer.

- The proposed device is capable of real-time stiffness measurements during cell culture studies through their mechanotransduction scheme (polymer substrate).
- The device can be redesigned and fabricated for a different range of measurements.
- The setup can be used reversely, (without stimulation) seeded cells mechanical contraction can be measured.

4.2.2 Our Device Results Compared to Instron Results

The comparison of results shown in chart 3 (a-d) displays similarities in some compositions and variations in others, similarities in stiffness measurements were expected when testing conditions are the same, which occurred in PCL:CA 95:5 group where measured stiffness matched (0.58 N/mm). On the other hand, variations occur for some other reasons such as:

- **Presence of media during the test**. Since instron 5544 uses vertical large grips, the setup did not allow placing a petri dish with a media during tests. On the other hand, our device has a horizontal setup and allowed placing a petri dish for culturing media during tests. Moving samples out of culturing media to testing grips, or being not immersed in the media during the test is technically not considered a similar testing condition.
- **Elongation rate difference**, Instron machine does the mechanical test over a larger elongation range compared to our device.
- **Polymer substrate installation difference**. Our device used a polymer installation and cutter blade kit, while instron tested specimens were cut using markers and blades to match dimensions.

- **Comparison insufficiency,** the results obtained from instron tests showed a lot of error in the initial readings, the reason behind that was difficulty of wet substrate alignment in addition to a tiny griper shake. Comparing our device results of low range to the obtained results from instron would not be a sufficient comparison since the first portion of instron results contain a lot of error while our device is mostly sensitive in that low range.

4.3 Future Work

- Conduct cell culture mechanical stimulation studies using the proposed device. We will grow target cells on polymer substrates with measured stiffness and apply external mechanical stimulation to confirm cells better differentiation. (46)*.

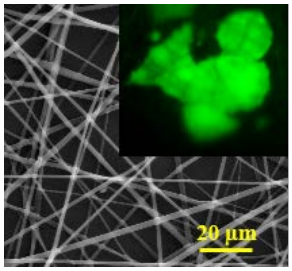

Figure 15: Nano fibrous scaffold (SEM micrograph) seeded with MCF-7 cancer cells showing cellular attachment to fibers (inset).*

- Use conductive polymer substrates to test different types of cultured cells and add gold electrodes for electrical stimulation.
- Custom embed piezoresistive sensors within 3D printed springs as (47) instead of microfabrication of metal springs; which will require adding a reflective surface in the middle of the spring to operate the laser-based optical sensing.
- Build remote arms to fit cantilever-based micro tweezer sensors for cell manipulation and stiffness characterization.
- Design and incorporate a media changing arrangement.
- Integrate the setup with a small microscope-friendly cell culture incubator.
- Combine the previous arrangements to build a microenvironment that can run longer experiments and support more bioanalysis features.

References

1. Lim C, Zhou E, Li A, Vedula S, Fu H. Experimental techniques for single cell and single molecule biomechanics. Materials Science and Engineering: C. 2006;26(8):1278-88.

2. Li Q, Lee G, Ong C, Lim C. AFM indentation study of breast cancer cells. Biochem Biophys Res Commun. 2008;374(4):609-13.

3. Crick S, Yin F. Assessing micromechanical properties of cells with atomic force microscopy: importance of the contact point. Biomechanics and modeling in Mechanobiology. 2007;6(3):199-210.

4. Lee GY, Lim CT. Biomechanics approaches to studying human diseases. Trends Biotechnol. 2007;25(3):111-8.

5. Guck J, Schinkinger S, Lincoln B, Wottawah F, Ebert S, Romeyke M, et al. Optical deformability as an inherent cell marker for testing malignant transformation and metastatic competence. Biophys J. 2005;88(5):3689-98.

6. Leung D, Glagov S, Mathews M. A new in vitro system for studying cell response to mechanical stimulation: different effects of cyclic stretching and agitation on smooth muscle cell biosynthesis. Exp Cell Res. 1977;109(2):285-98.

7. Rodbard S. Negative feedback mechanisms in the architecture and function of the connective and cardiovascular tissues. Perspect Biol Med. 1970;13(4):507-27.

8. McBeath R, Pirone DM, Nelson CM, Bhadriraju K, Chen CS. Cell shape, cytoskeletal tension, and RhoA regulate stem cell lineage commitment. Developmental cell. 2004;6(4):483-95.

9. Rajagopalan J, Saif MTA. MEMS sensors and microsystems for cell mechanobiology. J Micromech Microengineering. 2011;21(5):054002.

10. Engler AJ, Sen S, Sweeney HL, Discher DE. Matrix elasticity directs stem cell lineage specification. Cell. 2006;126(4):677-89.

11. Pelham RJ,Jr, Wang Y. Cell locomotion and focal adhesions are regulated by substrate flexibility. Proc Natl Acad Sci U S A. 1997 Dec 9;94(25):13661-5.

12. Yeung T, Georges PC, Flanagan LA, Marg B, Ortiz M, Funaki M, et al. Effects of substrate stiffness on cell morphology, cytoskeletal structure, and adhesion. Cell Motil Cytoskeleton. 2005;60(1):24-34.

13. Zheng J, Lamoureux P, Santiago V, Dennerll T, Buxbaum RE, Heidemann SR. Tensile regulation of axonal elongation and initiation. J Neurosci. 1991 Apr;11(4):1117-25.

14. Puig-De-Morales M, Grabulosa M, Alcaraz J, Mullol J, Maksym GN, Fredberg JJ, et al. Measurement of cell microrheology by magnetic twisting cytometry with frequency domain demodulation. J Appl Physiol (1985). 2001 Sep;91(3):1152-9.

15. Franze K, Gerdelmann J, Weick M, Betz T, Pawlizak S, Lakadamyali M, et al. Neurite branch retraction is caused by a threshold-dependent mechanical impact. Biophys J. 2009;97(7):1883-90.

16. Desmoulière A, Chaponnier C, Gabbiani G. Tissue repair, contraction, and the myofibroblast. Wound repair and regeneration. 2005;13(1):7-12.

17. Siechen S, Yang S, Chiba A, Saif T. Mechanical tension contributes to clustering of neurotransmitter vesicles at presynaptic terminals. Proc Natl Acad Sci U S A. 2009 Aug 4;106(31):12611-6.

18. Weiss L, Schmid-Schönbein GW. Biomechanical interactions of cancer cells with the microvasculature during metastasis. Cell Biophys. 1989;14(2):187-215.

19. Bao G, Suresh S. Cell and molecular mechanics of biological materials. Nature materials. 2003;2(11):715-25.

20. Suresh S, Spatz J, Mills J, Micoulet A, Dao M, Lim C, et al. Connections between single-cell biomechanics and human disease states: gastrointestinal cancer and malaria. Acta biomaterialia. 2005;1(1):15-30.

21. Van Vliet K, Bao G, Suresh S. The biomechanics toolbox: experimental approaches for living cells and biomolecules. Acta Materialia. 2003;51(19):5881-905.

22. GILLESPIE JS. Spontaneous mechanical and electrical activity of stretched and unstretched intestinal smooth muscle cells and their response to sympathetic-nerve stimulation. J Physiol. 1962 Jun;162:54-75.

23. Burnstock G, Holman ME. Autonomic nerve-smooth muscle transmission. Nature. 1960;187:951-2.

24. Burnstock G, Holman ME. The transmission of excitation from autonomic nerve to smooth muscle. J Physiol (Lond). 1961;155(1):115-33.

25. BURNSTOCK G, PROSSER CL. Responses of smooth muscles to quick stretch: relation of stretch to conduction. Am J Physiol. 1960 May;198:921-5.

26. Leung DYM, Glagov S, Mathews MB. A new in vitro system for studying cell response to mechanical stimulation. Exp Cell Res. 1977 15 October 1977;109(2):285-98.

27. Burchiel KJ. Effects of electrical and mechanical stimulation on two foci of spontaneous activity which develop in primary afferent neurons after peripheral axotomy. Pain. 1984;18(3):249-65.

28. Grigg P. Biophysical studies of mechanoreceptors. J Appl Physiol (1985). 1986 Apr;60(4):1107-15.

29. Sanderson MJ, Charles AC, Dirksen ER. Mechanical stimulation and intercellular communication increases intracellular Ca2+ in epithelial cells. Cell Regul. 1990 Jul;1(8):585-96.

30. Delbono O, Renganathan M, Messi ML. Regulation of mouse skeletal muscle L-type Ca2+ channel by activation of the insulin-like growth factor-1 receptor. J Neurosci. 1997 Sep 15;17(18):6918-28.

31. Tidball JG. Mechanical signal transduction in skeletal muscle growth and adaptation. J Appl Physiol (1985). 2005 May;98(5):1900-8.

32. Wong JY, Langer R, Ingber DE. Electrically conducting polymers can noninvasively control the shape and growth of mammalian cells. Proc Natl Acad Sci U S A. 1994 Apr 12;91(8):3201-4.

33. Folkman J, Moscona A. Role of cell shape in growth control. . 1978.

34. Ben-Ze'ev A, Farmer SR, Penman S. Protein synthesis requires cell-surface contact while nuclear events respond to cell shape in anchorage-dependent fibroblasts. Cell. 1980;21(2):365-72.

35. Ingber DE. Fibronectin controls capillary endothelial cell growth by modulating cell shape. Proc Natl Acad Sci U S A. 1990 May;87(9):3579-83.

36. Mooney D, Hansen L, Vacanti J, Langer R, Farmer S, Ingber D. Switching from differentiation to growth in hepatocytes: control by extracellular matrix. J Cell Physiol. 1992;151(3):497-505.

37. Ingber DE, Folkman J. Mechanochemical switching between growth and differentiation during fibroblast growth factor-stimulated angiogenesis in vitro: role of extracellular matrix. J Cell Biol. 1989 Jul;109(1):317-30.

38. Thilly WG. Mammalian cell technology. Butterworths; 1986.

39. Street G, Clarke T. Conducting polymers: a review of recent work. IBM Journal of Research and Development. 1981;25(1):51-7.

40. Kanatzidis MG. Conductive polymers. Chemical & engineering news. 1990;68(49).

41. Schmidt CE, Shastri VR, Vacanti JP, Langer R. Stimulation of neurite outgrowth using an electrically conducting polymer. Proc Natl Acad Sci U S A. 1997 Aug 19;94(17):8948-53.

42. Kim B, Nikolovski J, Bonadio J, Mooney DJ. Cyclic mechanical strain regulates the development of engineered smooth muscle tissue. Nat Biotechnol. 1999;17(10):979-83.

43. Discher DE, Janmey P, Wang YL. Tissue cells feel and respond to the stiffness of their substrate. Science. 2005 Nov 18;310(5751):1139-43.

44. Brown TD. Techniques for mechanical stimulation of cells in vitro: a review. J Biomech. 2000;33(1):3-14.

45. Bragança F, Rosa D. Thermal, mechanical and morphological analysis of poly (ε-caprolactone), cellulose acetate and their blends. Polym Adv Technol. 2003;14(10):669-75.

46. Jaiswal D, Brown JL. Nanofiber diameter-dependent MAPK activity in osteoblasts. Journal of Biomedical Materials Research Part A. 2012;100(11):2921-8.

47. Muth JT, Vogt DM, Truby RL, Mengüç Y, Kolesky DB, Wood RJ, et al. Embedded 3D printing of strain sensors within highly stretchable elastomers. Adv Mater. 2014;26(36):6307-12.